INFORMATION TO USERS

This manuscript has been reproduced from the microfilm master. UMI films the text directly from the original or copy submitted. Thus, some thesis and dissertation copies are in typewriter face, while others may be from any type of computer printer.

The quality of this reproduction is dependent upon the quality of the copy submitted. Broken or indistinct print, colored or poor quality illustrations and photographs, print bleedthrough, substandard margins, and improper alignment can adversely affect reproduction.

In the unlikely event that the author did not send UMI a complete manuscript and there are missing pages, these will be noted. Also, if unauthorized copyright material had to be removed, a note will indicate the deletion.

Oversize materials (e.g., maps, drawings, charts) are reproduced by sectioning the original, beginning at the upper left-hand corner and continuing from left to right in equal sections with small overlaps. Each original is also photographed in one exposure and is included in reduced form at the back of the book.

Photographs included in the original manuscript have been reproduced xerographically in this copy. Higher quality 6" x 9" black and white photographic prints are available for any photographs or illustrations appearing in this copy for an additional charge. Contact UMI directly to order.

Order Number 9312225

Supported metal clusters and cluster-substrate interaction
studied by scanning tunneling microscopy

Xhie, Jie, Ph.D.

University of Hawaii, 1992

U·M·I

SUPPORTED METAL CLUSTERS AND CLUSTER-SUBSTRATE
INTERACTION STUDIED BY SCANNING TUNNELING MICROSCOPY

A DISSERTATION SUBMITTED TO THE GRADUATE DIVISION OF THE
UNIVERSITY OF HAWAII IN PARTIAL FULFILLMENT OF THE
REQUIREMENTS FOR THE DEGREE OF

DOCTOR OF PHILOSOPHY

IN PHYSICS

DECEMBER 1992

By

Jie Xhie

Dissertation committee:
Klaus Sattler, Chairman
Charles S. Fadley
William Pong
Pui K. Lam
Frederick Harris

TO MY PARENTS

iii

ACKNOWLEDGMENTS

I would like to acknowledge my academic adviser, Prof. Klaus Sattler, for his encouragement, guidance and patience during the course of this study.

I am grateful to Dr. U. Müller for his help during my early stage of research. My colleagues, N. Venkateswaran, M. Ge, and G. Raina, also deserve recognition for their cooperation and support in the completion of this work.

My special appreciation goes to Prof. W. Pong for providing his laboratory facilities; Mr. J. F. Zheng and Mr. A. Rizzetti for preparing some of the samples.

ABSTRACT

This PhD dissertation is concerned with an experimental study of supported metal clusters and cluster-substrate interaction. The geometric and electronic structures of platinum and cobalt clusters on graphite, the effects of clusters on the graphite substrate, and the influences from the substrate to clusters were investigated by scanning tunneling microscopy.

A topographic study of adatoms and small clusters of platinum and cobalt on highly-oriented pyrolytic graphite was performed both in air and in ultra-high vacuum. The samples were prepared by vapor deposition on the graphite surface. Stable images of adatoms and small clusters on graphite were obtained with atomic resolution showing their atomic structures. Taking the graphite lattice as reference, the adsorption sites of adatoms and clusters on the surface as well as the bond lengths and bond angles of clusters were determined.

Various superstructures on graphite were found near the adsorbed clusters, or generally near defects. The superstructures are localized in small areas near the clusters and decay within a distance of 2 - 5 nm into the graphite lattice. Detailed analyses show that they were due to periodic charge-density modulations superimposed onto the graphite lattice. The different periodic modulations have the same period of 1.5a (a = 0.245 nm, is the lattice constant of graphite) and exist in three possible directions, each rotated 30° relative to the graphite lattice. They are generated by adsorbed clusters which act as a scattering center and perturb the surface charge-density.

Among many graphite substrates being studied, anomalous giant lattices were observed on three of the samples. They exhibited hexagonal

symmetry with lattice constants of 1.7 nm, 2.8 nm, 3.8 nm and 6.6 nm. Atomic resolution of graphite was obtained simultaneously. By introducing small rotations of the top graphite layer relative to the underlying single crystal, a complete description is developed to account for all the features displayed by the STM images. In addition to the giant and atomic lattices, a supergiant lattice was observed. Cobalt particles on the surface were also imaged and were found on the top sites of the giant lattice.

TABLE OF CONTENTS

LIST OF FIGURES

LIST OF ABBREVIATIONS

CDW   Charge-Density Waves

EXAFS   Extended X-ray Adsorption Fine-Structure

FIM   Field Ion Microscopy

HOPG   Highly Oriented-Pyrolytic Graphite

HV   High Vacuum

LDOS   Local Density Of States

PCDM   Periodic Charge-Density Modulation

PLD   Periodic Lattice Distortions

STM   Scanning Tunneling Microscopy

TEM   Transmission Electron Microscopy

UHV   Ultra-High Vacuum

XPS   X-ray Photoelectron Spectroscopy

Chapter I

INTRODUCTION

Since the development of new cluster sources in the early 80's and their combination with mass spectrometry and electron spectroscopy techniques, cluster science has become a rapidly increasing and fascinating research field. Clusters of atoms have been studied in beams, on substrates, or isolated in inert matrices. Various new properties have been found for such small atomic systems due to their unique structures and the quantum confinement of the valence electrons.[1-4]

Most of the work in recent years has been concentrated on free clusters in molecular beams. Clusters in beams do not interact with each other or with other materials, and therefore their intrinsic properties can be investigated. However, for most of the experiments the clusters have to be ionized prior to their investigation and the properties of the electrically neutral particles are hardly accessible. Also, most of the studies on free clusters are accompanied by fragmentation events which often complicate data interpretation.

From the surface and material sciences point of view, the understanding of small atomic clusters adsorbed on solid substrates is of fundamental importance. The static and dynamic behavior of supported clusters form the basis for many applications, for example thin film formation, microelectronics processing and so on. In particular, nucleation and growth studies in the early stages can lead to new processes for improved material characteristics.

1.1   Specific Problems of the Dissertation

This dissertation deals with two specific problems: (1) to obtain the atomic structure of small metal clusters deposited on solid supports; (2) to observe the interaction of adsorbed clusters with the substrate.

To investigate the atomic structures of metal clusters deposited on graphite, single clusters have to be imaged individually with atomic resolution. Also, the atomic lattice of the substrate has to be obtained simultaneously in order to determine how the clusters are arranged relative to the atoms of the substrate.

The interaction of an adsorbed cluster with the substrate can have two effects: the substrate determines the adsorption site and arrangement of the cluster; and the cluster alters the local structure of the substrate.

For both problems of interest, knowledge of the atom by atom arrangement is of fundamental importance. However, such knowledge can be very difficult to acquire from an experimental point of view, because most surface structure techniques used today do not have the ability to study individual surface atomic sites. The field ion microscopy (FIM) has been applied to study the diffusion of single adatoms and the growth of clusters containing a few atoms,[5] while the geometrical structures of larger clusters have been determined by transmission electron microscopy (TEM).[6] Both microscopic techniques have several disadvantages for cluster work: FIM is restricted to strongly interacting substrates, small clusters and relatively small observation areas; TEM is restricted to large clusters and it can heat up the clusters. Therefore, for our purpose of study we must turn to other techniques.

1.2   Experimental Approach to the Problems

1.2.1 Scanning Tunneling Microscopy

The recently developed scanning tunneling microscope (STM) is a unique and promising device for cluster research. It provides direct, real space images of surface topography, both periodic and nonperiodic, on the atomic scale. It can be operated in air, in liquids or under ultra-high vacuum conditions. Metal clusters on weakly interacting substrates can then be directly imaged. The STM can be applied within a broad size range from single adatoms to particles with diameters of hundreds of angstroms.[7] It yields the morphologies of clusters and furthermore shows how they are registered relative to the substrate lattice.[7, 8]

The principle of the STM is quite simple. A small metal tip is brought near enough, typically a few angstroms, to a conducting surface that the vacuum tunneling resistance between surface and tip is finite and measurable (Figure 1.1). A small voltage is then applied between the tip and sample, encouraging electrons to quantum mechanically tunnel across the gap. An image can be formed by rastering the tip across the surface (in the X and Y plane), while moving the tip in the Z direction (perpendicular to the surface) to maintain a constant tunneling resistance. As a result, the Z motion of the tip represents essentially a contour map of the surface. This is called the height mode or constant current mode as shown in Figure 1.2(a).

An alternative method of image formation is to raster the tip rapidly across the surface at a constant average height, and changes in the tunneling current constitute the image.[9] This is called the current mode or

constant height mode as shown in Figure 1.2(b). For a flat surface, this imaging mode has the advantage of higher speed and lower noise.

The atomic resolution of the STM is due to the very strong dependence of the tunneling current on the gap between tip and sample. For electronic states at the Fermi level, the surface can be represented as a potential barrier whose height is equal to the work function ϕ. The tunneling current varies exponentially with the vacuum gap distance. The decay length is $h(8m\phi)^{-1/2}/2\pi$, where h is Plank constant and m is the mass of electron. For typical metallic work functions, this length is ~ 0.04 nm. Thus, in the constant current mode, the tip may be expected to follow the surface height to 0.01 nm or better.

To arrive at an explicit expression for the tunneling current, many approximations have to be made. Tersoff and Hamann[10] have developed a theory of STM based on Bardeen's formalism[11] for tunneling current. In their work, the surface is treated exactly while the tip is modeled as a locally spherical potential well where it approaches nearest the surface. Realistically, the sharpest tip imaginable is a single atom supported on a cluster or small plateau. At room temperature and at small bias voltage, the tunneling current is found to be

$$I = 64\pi^4 h^{-1} e^2 V \phi^2 D_t(E_F) R^2 \kappa^{-4} e^{2\kappa R} \times \sum |\varphi_v(r_o)|^2 \delta(E_v - E_F) ,$$

where: e is the electric charge of electron; V is the bias voltage; $D_t(E_F)$ is the density of states at the Fermi level per unit volume of the probe tip; R is the local radius of curvature of the tip about the center located at r_o; $\kappa = 2\pi(2m\phi)^{1/2}/h$ is the inverse decay length for wave functions in vacuum; and $\varphi_v(r_o)$ is the surface wave function at position r_o. The summation on the right side of the equation is simply the surface local density of states (LDOS) at E_F at the position of the tip.

For arbitrarily localized metal tips, the density of states at the Fermi level, $D_t(E_F)$, is constant. Thus, the tunneling current is proportional to the local density of states of the surface at the position of the tip:

$$I \ \alpha \ \sum |\varphi_v(r_o)|^2 \ \delta(E_v - E_F) \, .$$

Based on analogy with the one-dimensional tunneling problem,[12] $|\varphi_v(r_o)|^2$ is proportional to $e^{-2\kappa(R+d)}$, where d is the separation between tip and sample. Therefore we see that the tunneling current decays exponentially with the tip-sample separation. This gives the remarkable sensitivity of the STM to study the surface topography of any electrically conducting sample.

Since the tunneling current is related to not only the tip-sample separation but also the surface density of states at the Fermi level, the STM images essentially display a mixture of the geometric and electronic strucure of the surface. This complicates the interpretation of images that one has to always take into accout both effects.

In order to obtain atomic resolution images of metal clusters on surfaces, the STM has to operate under optimal conditions concerning thermal drift, vibration isolation, and electronic performance. This is because the surface atoms of metals are known to show very small height corrugations.

1.2.2 Sample Preparation Method

For our studies of supported metal clusters, the samples have been prepared by depositing the metal onto the (0001) surface of highly-oriented pyrolytic graphite (HOPG). More specifically, a tungsten wire was used as the heating element and a small strip of deposition material was wrapped on it. Then it was placed about 10 cm away from the substrate and was

heated by applying a current through the filament. As soon as the deposition material started evaporating, we turned off the current so that only a small amount of material was deposited onto the substrate. Metal clusters are formed after deposition with subsequent diffusion and growth on the surface.[13]

Using graphite as the substrate is convenient for this study because: it is easily cleaved to give atomically flat surfaces over relatively large areas; it is chemically inert and can be imaged with atomic resolution to serve as a reference.

A schematic drawing of the structure of graphite is illustrated in Figure 1.3. It consists of planes of carbon atoms, each forming a honeycomb structure, stacked in a manner such that half of the carbon atoms (α atoms) are located directly above atoms in the adjacent plane, while the other half (β atoms) are located above the center of the honeycomb in the adjacent plane.[14] The lattice constant of graphite, the distance between two nearest β atoms, is 0.2456 nm. Carbon atoms within a layer are strongly bonded while the interaction between layers are much weaker. This allows the material to be easily cleaved.

1.2.3 Experimental Setup

The main instrument for our study is a scanning tunneling microscope. It can be operated with two different scanning heads; one is designed for operation in air[15] and the other for operation in ultra-high vacuum (UHV).[16] The STM system, NanoScope II,[15] contains three major parts: microscope, control unit and computer workstation. Figure 1.4 is a schematic of NanoScope II. The microscope consists of a tunneling tip attached to a piezoelectric tube, a sample holder and a stepper motor. The

control unit is an analog/digital interface system acting as a gateway between the computer workstation and the microscope. The computer workstation consists of a 80386 PC/AT-compatible computer, a color graphics monitor and a monochrome text monitor. The basic function of the instrument is to move the tip in an X-Y raster scan across a conducting sample while sensing the tunneling current between the tip and sample. A feedback loop is used to control the height of the tip by applying a voltage to the scanning piezo.

An ultra-high vacuum system has been built for accommodation of the UHV-STM. Attached to it is a high vacuum (HV) sample preparation system ($\sim 10^{-8}$ Torr). This allows us to keep the main chamber in the range of 10^{-11} - 10^{-10} Torr while new substrates and deposition materials are introduced into the preparation chamber. It also keeps the main chamber clean during the deposition. Single crystals, especially layered materials such as graphite, can be cleaved in vacuum to give clean surfaces for cluster formation.

Figure 1.5 is a schematic drawing of the top view of our UHV-HV system. The UHV and HV chambers are connected by a straight-through valve. The UHV-STM is mounted on one of the flanges in the main chamber. Samples are prepared in the HV chamber and then transferred into the UHV chamber by a long feedthrough without breaking the vacuum. A manipulator is also mounted to the main chamber to transport sample between the STM and the sample holder attached to the long feedthrough.

Some of our samples were prepared in Prof. Pong's laboratory.[17] The same sample preparation method was applied under similar conditions as those described in section 1.2.2.

1.3 References

1. E. R. Hilf, F. Kammer and K. Wien, "PDMS and Clusters," Springer (1986).

2. F. Traeger and G. zu Putltz, "Metal Clusters," Springer (1986).

3. P. Jena, B. K. Rao, and S. N. Khanna, "Physics and Chemistry of Small Clusters," NATO ASI Series B: Physics Vol. **158**, Plenum Press (1987).

4. S. Sugano, Y. Nishina, and S. Ohnishi, "Microclusters," Springer Series in Materials Science **4**, Springer (1987).

5. G. L. Kellog, Surf. Sci. **187**, 153 (1987).

6. S. Iijima and T. Ichihashi, Phys. Rev. Lett. **56**, 616 (1986).

7. E. Ganz, K. Sattler, and J. Clarke, J. Vac. Sci. Technol. A **6**, 419 (1988).

8. E. Ganz, K. Sattler, and J. Clarke, Phys. Rev. Lett. 60, 1856 (1988); ibid. Surf. Sci. **219**, 33 (1989).

9. D. P. E. Smith and S. Elrod, Rev. Sci. Inst. **56**, 1970 (1985).

10. J. Tersoff and D. R. Hamann, Phys. Rev. B **31**, 805 (1985).

11. J. Bardeen, Phys. Rev. Lett. **6**, 57 (1961).

12. G. Binnig, H. Rohrer, Ch. Gerber, and E. Weibel, Phys. Rev. Lett. **49**, 57 (1982).

13. J. A. Venables, J. Derrien, and A. P. Janssen, Surf. Sci. **95**, 441 (1980).

14. D. Sands, "Introduction to Crystallography," Benjamin-Cummings, Reading, Mass., (1969).

15. Digital Instruments, Inc., Santa Barbara, CA, USA.

16. McAllister Technical Services, Coeur d'Alene, Idaho, USA.

17. W. Pong, Department of Physics, University of Hawaii at Manoa.
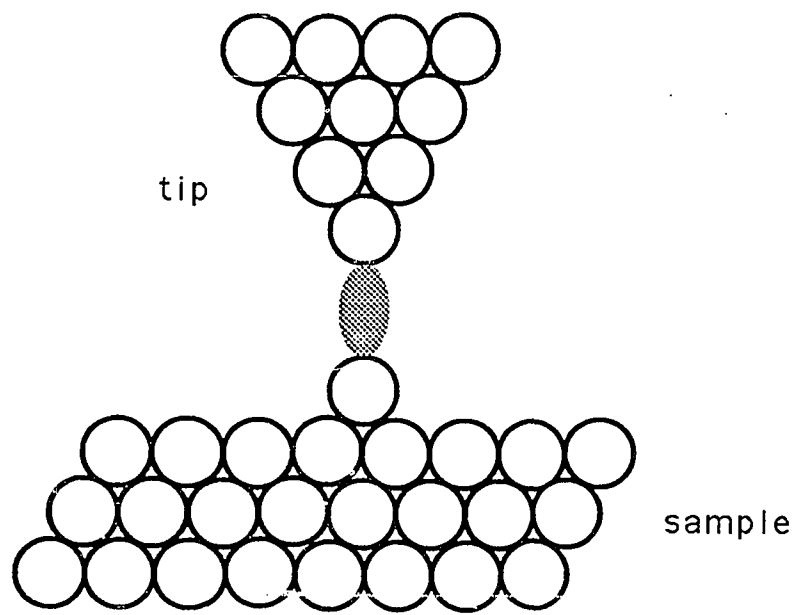
Figure 1.1: Principle of the STM. The tunneling current flows in between two nearest atoms of the tip and the sample.

(a) constant current mode

tip

current

bias voltage V

sample

(b) constant height mode

tip

d

current

bias voltage V
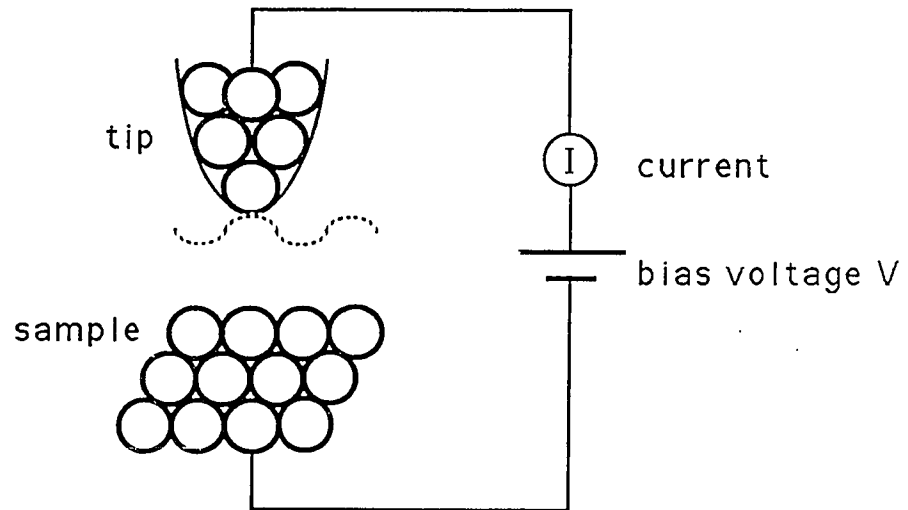
sample
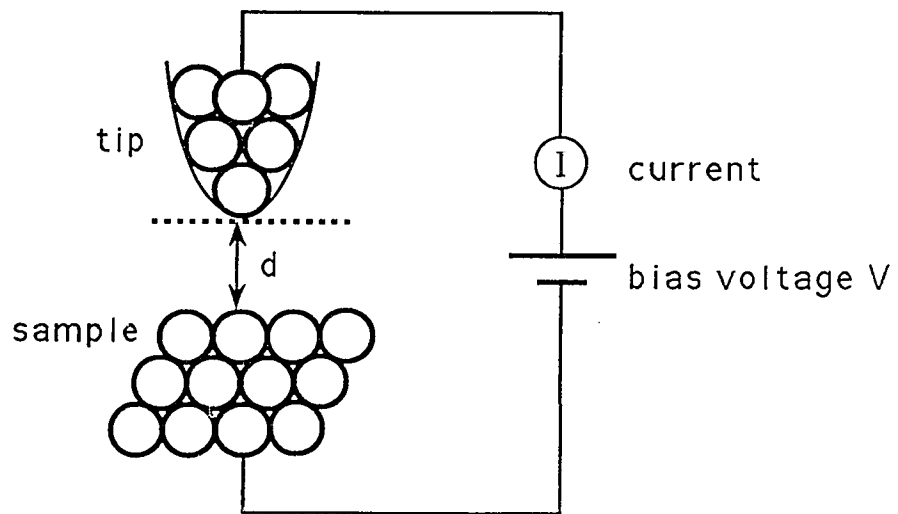
Figure 1.2: Two operational modes of the STM.

10

α atom

β atom

a: 0.2456 nm
c: 0.6696 nm
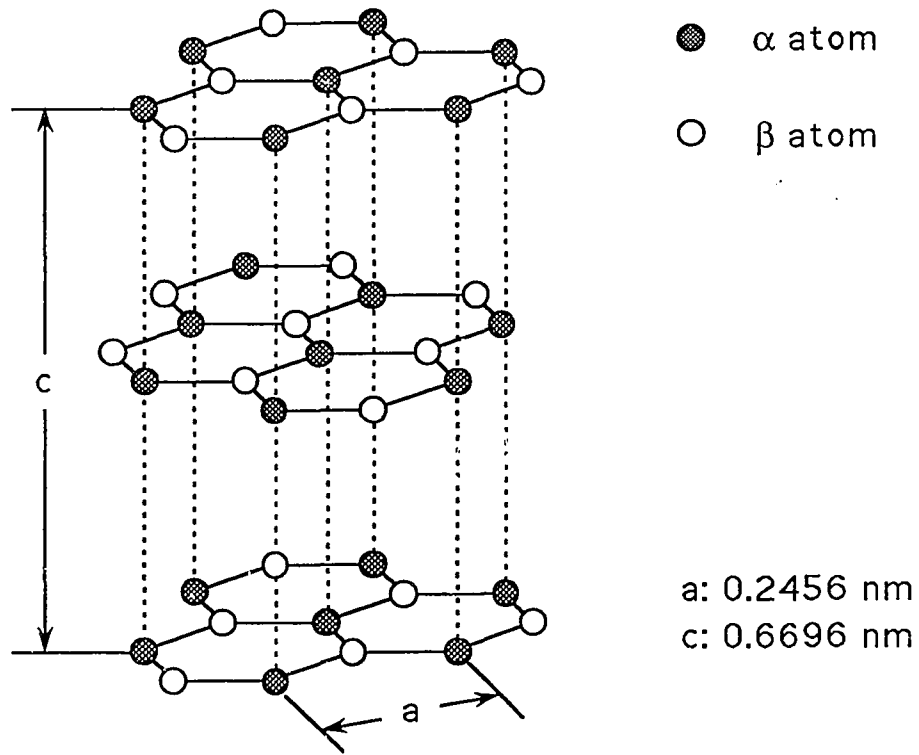
Figure 1.3:   Schematic drawing of graphite structure

11
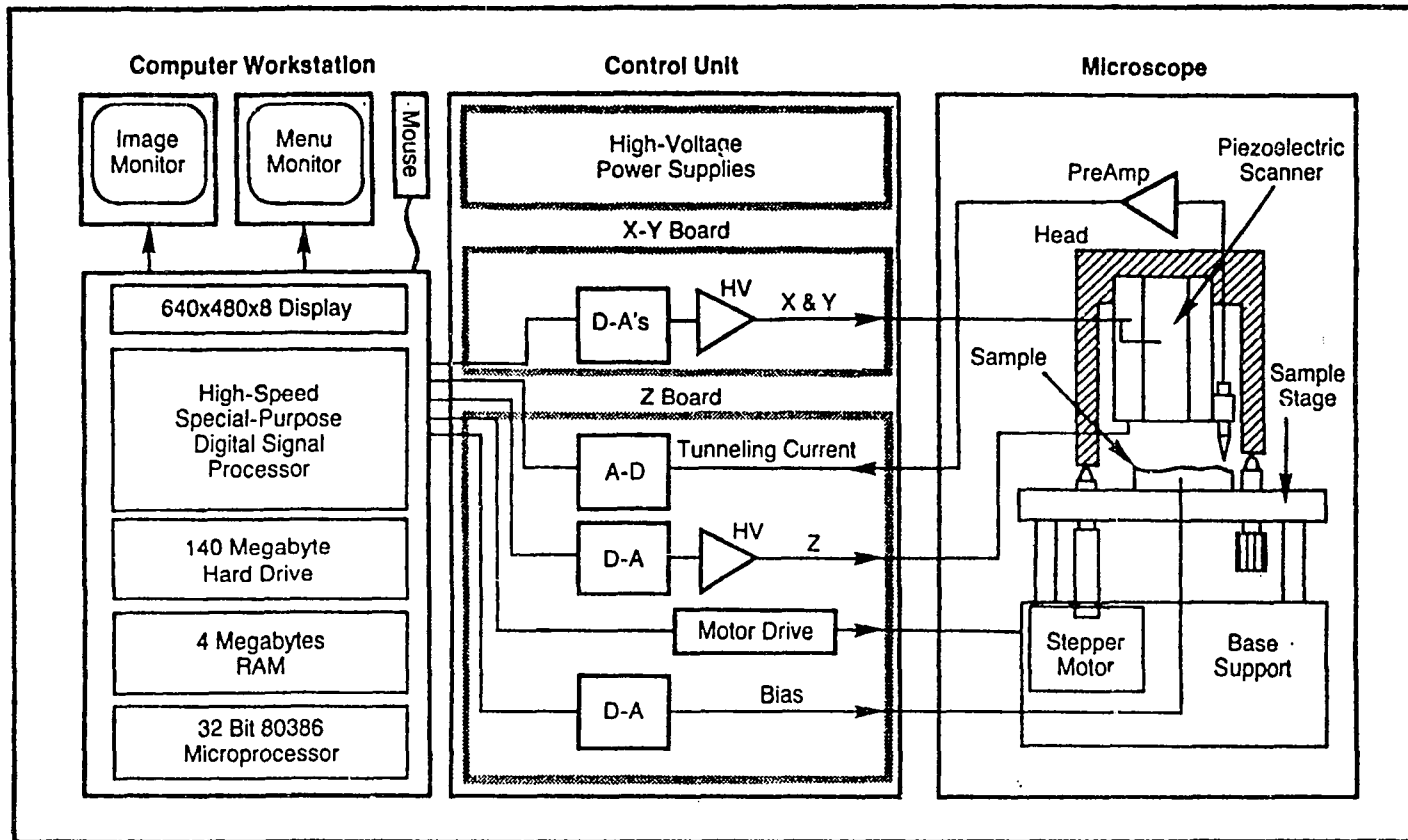
Figure 1.4: A schematic of Nanoscope II
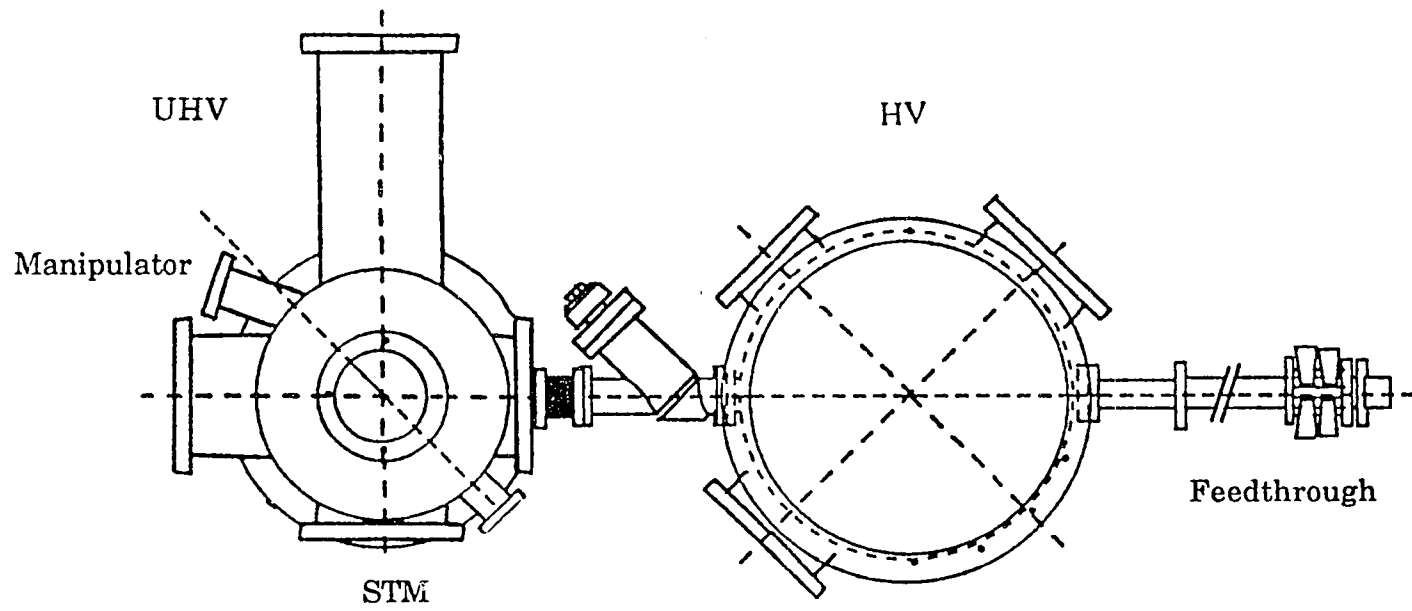
Figure 1.5: Top view of the UHV-HV system.

Chapter II

**SCANNING TUNNELING MICROSCOPY OF PLATINUM ADATOMS
AND SMALL CLUSTERS ON GRAPHITE**

2.1   Introduction

The formation of clusters on single crystal substrates plays an important role in the nucleation and growth processes of thin films. Surface and interface research often has to take into account the microscopic features and morphology dynamics occurring in the early stages of film formation. In the submonolayer regime, adatoms can acquire various positions on top of the substrate lattice and the question of commensurate or non-commensurate arrangements is of fundamental importance. Clusters, containing just a few atoms can be the nuclei for film growth and their initial structures can determine the final film quality.

A few studies have been reported during recent years using STM for cluster and granular film research. Small Si clusters were imaged on a Au(001)-(5×20) reconstructed surface and current-voltage characteristics were taken revealing the cluster energy band gap.[1] An STM/STS analysis of Fe particles on GaAs showed a size dependent metal-insulator transition.[2] Sb clusters on GaAs were formed for coverages in the range of a few percent of a monolayer.[3] As the coverage was increased, the Sb islands were growing in size while maintaining a height corresponding to one monolayer. Then, for coverages close to one monolayer, the Sb islands formed a continuous monolayer. Planar clusters have also been imaged for

Cr/GaAs(110).[4] Preferential clustering along step edges was observed in this case. The mechanism for the formation of small clusters on GaAs(110) has been discussed in terms of the adatom-substrate interaction, in particular, the pairing of Au-adatoms.[5] A metastable 3D cluster phase was found for Ge on Si(001) with clusters having a {105} ordered structure.[6]

Cluster imaging with the STM for obtaining atomic structures is mainly limited to two-dimensional structures because the STM is only sensitive to the first atomic layer of the surface. Atoms in the center of a cluster are hidden from view. However, for very small clusters containing up to about 10 atoms, individual atoms can be imaged and bond lengths and angles can be determined. For weakly interacting substrates, small clusters of Cu, Ag, Au, and Al were analyzed on graphite with static and dynamic behavior being observed.[7] In this study, only a few small clusters were found which did not allow one to establish a statistical analysis.

Many calculations on bond lengths, bond angles and binding energies have been done for small free clusters.[8,9] However, only a few experimental data are available for comparison. The experimental data for nearest neighbor distances available so far were mostly obtained by extended x-ray-adsorption fine-structure (EXAFS) studies of clusters isolated in solid argon[10, 11, 12] or on amorphous carbon substrates.[13] Even in the most recent study the bond lengths for small clusters with more than two atoms were put together under the notion of multimers,[12] because they were obtained from a distribution of cluster sizes.

In this chapter we present a topographic study of platinum clusters on the surface of graphite. We show atomic resolution images of single platinum adatoms and small clusters of up to 8 atoms in a cluster. Different isomeric structures were found for clusters of one size. Taking

the graphite lattice as reference we determine, on a statistical basis, the adsorption sites of platinum single atoms as well as bond lengths for platinum dimers and trimers.

2.2   Experiment

Most of the samples were prepared in a high vacuum (10^{-7} torr) chamber by vapor deposition of platinum on freshly cleaved graphite substrates. A small strip of platinum wrapped on a tungsten filament was placed about 10 cm away from the substrate and a current of 45 A was applied to the filament. A few seconds after the platinum started evaporating we turned off the current so that only a small amount of platinum was deposited onto the substrate. After deposition the sample was analyzed by x-ray photoelectron spectroscopy (XPS), which showed a coverage of 2-4% of a platinum monolayer on the graphite surface. The samples were then transferred to a STM[14] working in air at room temperature. The STM images were taken within the first two days after preparation although the samples were stable for at least a week. Both constant current and constant height modes were used to obtain stable images with atomic resolution. The tunneling current was kept in the range of 1 - 21 nA and the tip bias voltage in the range of 3 -130 mV.

One of the samples was prepared in a similar way but in a different vacuum system. The graphite substrate was cleaved in a high vacuum (2×10^{-8} torr) chamber and a small amount of platinum was deposited onto the surface by thermal evaporation, similar as for the other samples. Then the sample was transferred to a STM,[15] mounted in an ultra-high vacuum (5×10^{-10} torr) chamber, without breaking vacuum. The images were

obtained in constant height mode in ultra-high vacuum at room temperature using a Pt-Ir tip. The tunneling current was kept in the range of 2 - 7 nA and the tip bias voltage in the range of 100 - 165 mV.

2.3   Results and Discussion

2.3.1 Imaging of Platinum Adatoms and Small Clusters

All the images presented in this chapter were quite stable for at least a few subsequent scans. This indicates that the diffusion of platinum clusters on the graphite surface is unlikely at room temperature.

Figures 2.1 (a) - (d) show four STM images of single platinum atoms on the surface of graphite. In (c) and (d), two atoms are shown in each image. Since they are well separated we consider them as two single atoms. The underlying graphite atomic lattice is imaged simultaneously and defines the adsorption sites of platinum atoms. As can be seen from the images, the atoms have a tendency to locate on top of β-sites of the graphite lattice, for example, (a) and (c). However, other adsorption sites are also possible.

In Figures 2.2 (a) - (d) we show four images of different platinum dimers on graphite. The bond distances of the dimers are very close to the lattice constant of graphite, 0.245 nm. The dimer in (a) lies along one of the graphite directions while the dimers in (b) - (d) are rotated up to 25° relative to the graphite lattice.

Figures 2.3 (a) - (c) display three platinum trimers of different structures. Schematic drawings of the structures of these trimers together with the underlying graphite lattice are displayed in (d) - (f). The trimers in (a) and (b) show a nearly equilateral structure and the trimer in (c) shows a

17

nearly linear structure. In the case of two equilateral trimers, the graphite surface in the nearby region is disturbed differently. In (a) the nearby graphite shows a large triangular shadow, while in (b) a superstructure is formed near the trimer. Such effects of clusters on the graphite substrate will be discussed in the next chapter.

Figures 2.4 (a) - (c) show three structures of platinum tetramers. Schematic drawings of the structures are displayed in (d) - (f). The tetramer in (a) shows a Z pattern with each platinum atom on top of a β-site. In (b) and (c) the tetramers are formed by a linear chain of three atoms along the graphite direction with the other atom attached to the side.

Figures 2.5 (a) - (c) display three structures of platinum hexamers and their schematic drawings are shown in (d) - (f). The hexamer in (a) is formed by a linear chain of four atoms along the graphite orientation with the other two atoms attached to the sides. In (b) and (c) the hexamers show more closed-packed structures. The alignment of atoms in these two clusters, however, are quite different. In (b) the atoms are aligned along directions which are rotated ~30° relative to the graphite lattice, while in (c) the atoms are aligned along the graphite orientation with each atom sitting on top of β-sites.

Figure 2.6 (a) shows an octamer with its structural model displayed in (b). The octamer is formed by two parallel arrays of four atoms oriented along the direction which is rotated ~30° with respect to the graphite lattice. The center four atoms show higher intensity and appear further apart than those at corners. This indicates that the octamer may no longer be a planar cluster. A suggested structure of the octamer is shown in (c), where a side view of the cluster is given. In this case, only the four atoms at the corners are bonded to the underlying graphite.

2.3.2 Adsorption Site and Bond Length Distributions

Since we have obtained a large number of images of different platinum single atoms, dimers and trimers, we are able to study their adsorption sites and bond lengths statistically. For such analyses, the underlying graphite lattice was used for calibration by choosing 30 - 40 points as reference for the lattice and calculating the lattice parameters by a least square fit to these lattice points. This procedure compensates for decalibration of the instrument and distortions caused by thermal drift is compensated. The lattice was calculated in two different ways, one with the hole-sites and the other with the β-sites as reference points. The position of a platinum atom was then determined by its peak in relation to the graphite lattice. The width of the atomic peak at a height of 75% above the mean height of the reference hole-sites was used as a measure for the uncertainty of the peak location. The bond lengths were measured peak to peak.

A statistical study of adsorption sites for platinum single atoms on graphite is performed by analyzing the positions of 70 platinum atoms relative to underlying graphite. Figure 2.7 shows the adsorption site distribution of the probability for a platinum atom adsorbed on the graphite surface. A triangle which can represent every adsorption site on the graphite lattice is used for the mapping of the probability distribution. As shown in the figure, the adsorption probability near a β-site, 36.2%, is about twice the probability near a hole-site or an α-site. There is also a 26.4% probability that an atom sits in between all three sites. Therefore a platinum atom has a fairly high tendency to bind to a β-site, but is quite free to bind to somewhere else.

19

In Figure 2.8 we show bond length distribution curves for platinum dimers and trimers. Each measured bond length was broadened using Gaussian function with the uncertainty as the width of the Gaussian function and added for all dimers and trimers, respectively. Each point on the curves gives the probability in percentage of the measured corresponding bond length in an interval of 0.001 nm.

For dimers the average bond length is 0.246 nm with a standard deviation of 0.026 nm. This value is very close to the lattice constant of graphite, indicating that the graphite surface may interfere and influence the bond distance of a dimer. However, this seems to be in contradiction to the relatively free choice of the adsorption site of the monomers. Also the broad distribution also suggests that the bond length may not be related to the graphite lattice constant. There are no data available on the bond distance of free platinum dimers so that no comparison can be made.

The average bond length for trimers is 0.261 nm with a standard deviation of 0.032 nm. This bond length is larger than the graphite lattice constant but smaller than the nearest neighbor distance, 0.277nm, of platinum in bulk.[16]

2.4   Conclusions

We have imaged platinum adatoms and very small clusters containing up to eight atoms in a cluster with atomic resolution. Cluster structures as well as their orientational and positional registry with the graphite lattice are determined. Different structures have been found for clusters of one size.

In addition a statistical study has been performed to obtain distributions of adsorption sites and bond lengths. We find that a platinum single atom tends to bind to the β-site of the graphite lattice, but has also a high probability to bind to any other sites. For dimers the average bond distance is 0.246 nm which is very close to the graphite lattice constant. The trimer bond length is 0.261 nm, suggesting that the Pt-Pt interaction is dominant.

2.5   References

1. Y. Kuk, M. F. Jarrold, P. J. Silverman, J. E. Bower, and W. L. Brown, Phys. Rev. B **39**, 11168 (1989).

2. P. N. First, J. A. Stroscio, R. A. Dragoset, D. T. Pierce, and R. J. Celotta, Phys. Rev. Lett. **63**, 1416 (1989).

3. P. Martensson and R. M. Feenstra, J. Microsc. **152**, 761 (1988).

4. B. M. Trafas, D. M. Hill, P. J. Benning, G. D. Waddill, Y.-N. Yang, R. L. Siefert, and J. H. Weaver, Phys. Rev. B **43**, 7174 (1991).

5. G. Allan and M. Lannoo, Phys. Rev. Lett. **66**, 1209 (1991).

6. Y.-W. Mo, D. E. Savage, B. S. Swartzentruber, and M. G. Lagally, Phys. Rev. Lett. **65**, 1020 (1990).

7. E. Ganz, K. Sattler, and J. Clark, Surf. Sci. **219**, 33 (1989).

8. T. H. Upton, Phys. Rev. Lett. **56**, 2168 (1986).

9. K. Raghavan, M. S. Stave, and A. E. DePristo, J. Chem. Phys. **91**, 1904 (1989).

10. P. A. Montano, W. Schulze, B. Tesche, G. K. Shenoy, and T. I. Morrison, Phys. Rev. B **30**, 672 (1984).

11. P. A. Montano, G. K. Shenoy, E. E. Alp, W. Schulze, J. Urban, Phys. Rev. Lett. **56**, 2076 (1986).

12. P. A. Montano, J. Zhao, M. Ramanathan, G. K. Shenoy, W. Schulze, and J. Urban, Chem. Phys. Lett. **164**, 126 (1989).

13. G. Apai, J. F. Hamilton, J. Stohr, and A. Thompson, Phys. Rev. Lett. **43**, 165 (1979).

14. Digital Instruments, Inc., Santa Barbara, CA, USA.

15. McAllister Technical Services, Coeur d'Alene, Idaho, USA.

16. C. Kittel, "Introduction to Solid State Physics," John Wiley & Sons, Inc., p23 (1986).
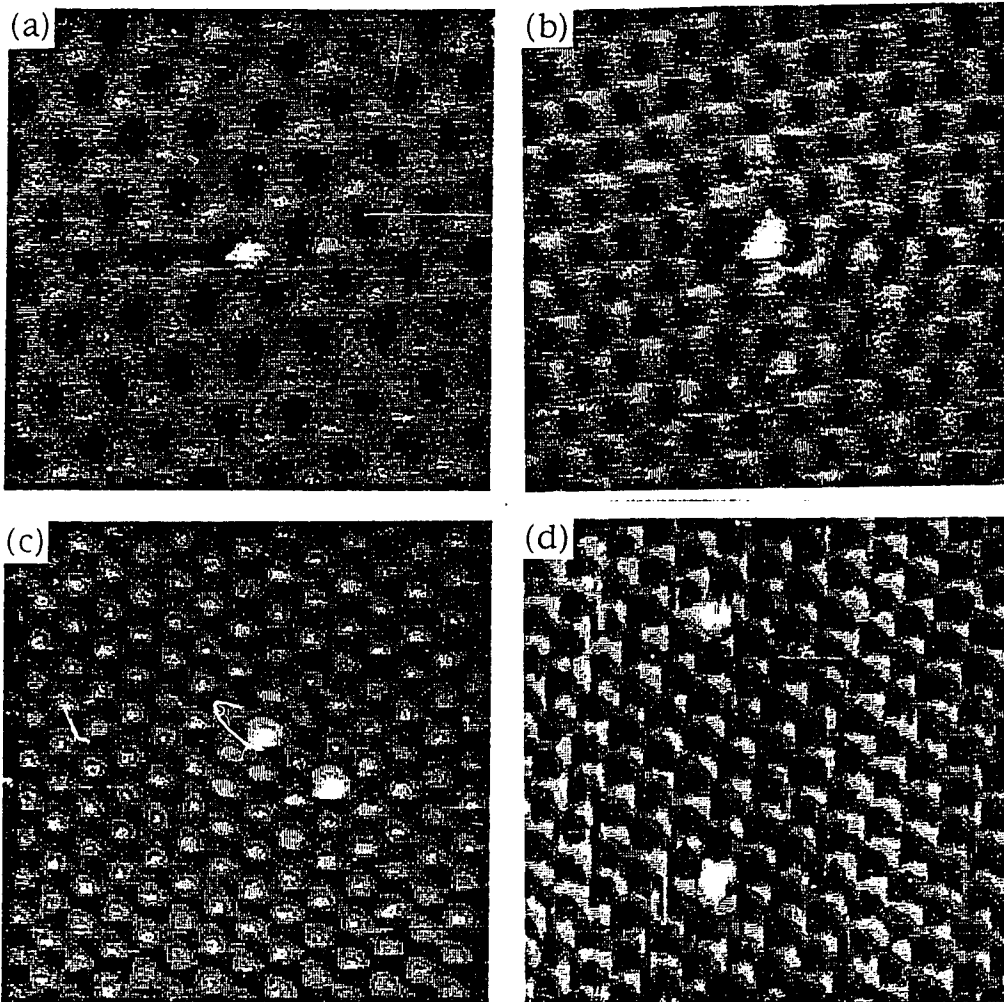
Figure 2.1: STM images of single platinum atoms on graphite.
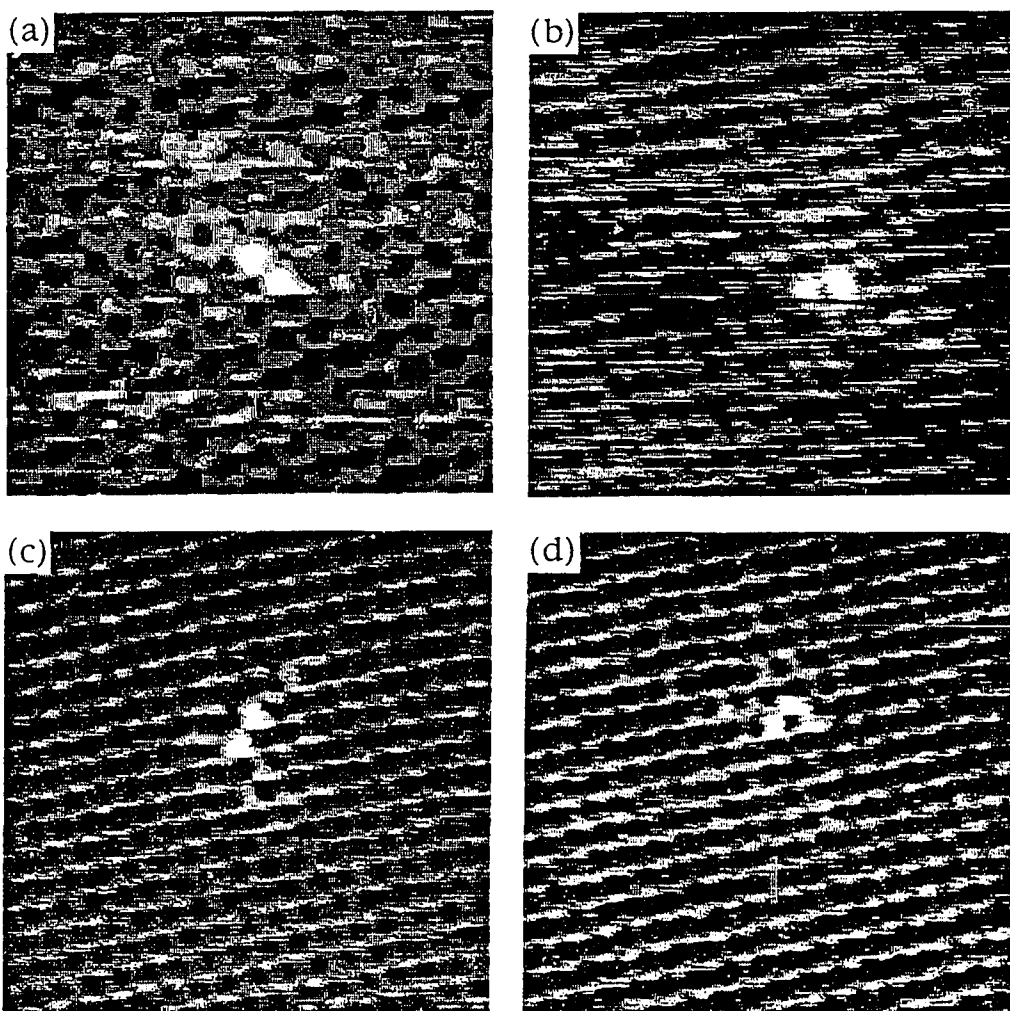
Figure 2.2: STM images of platinum dimers on graphite.
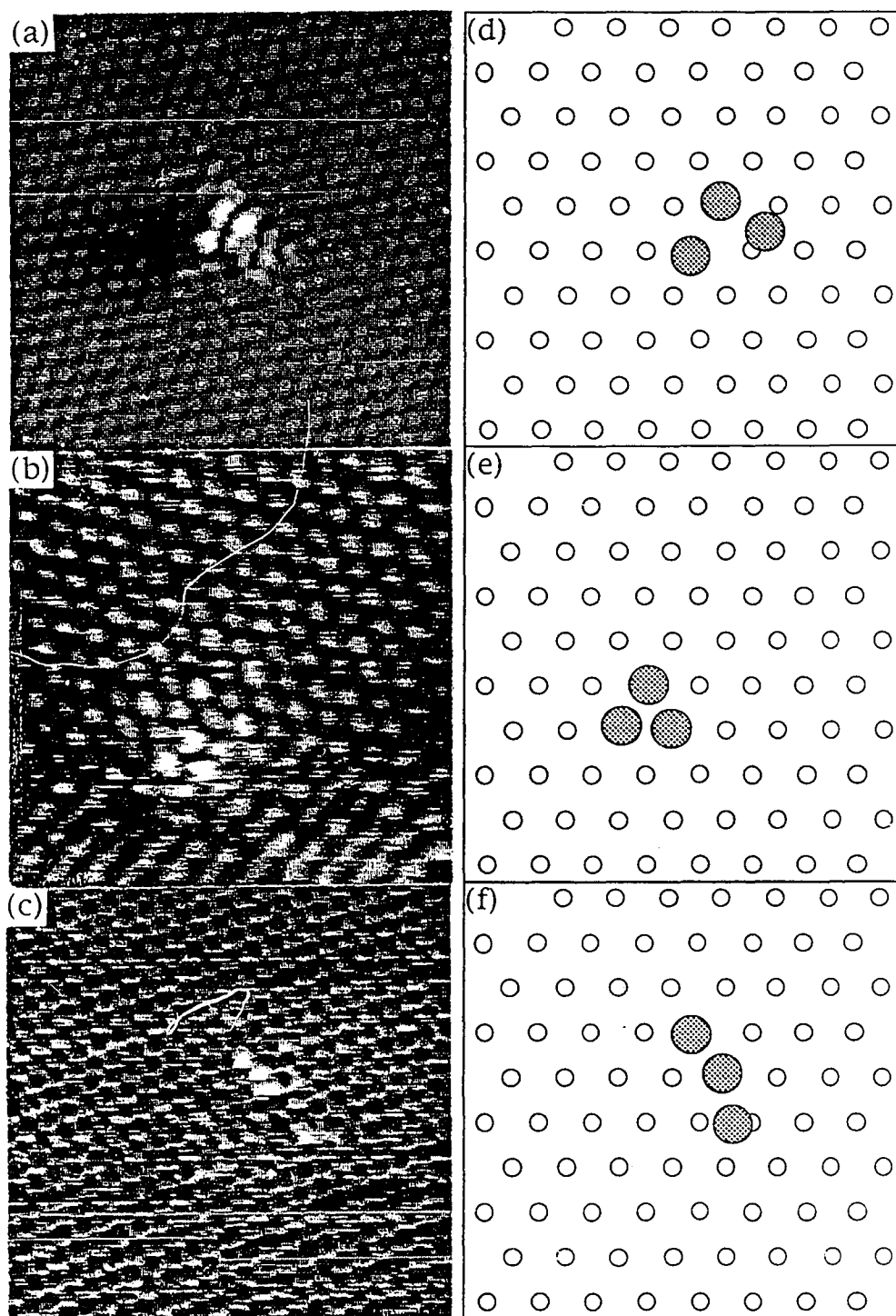
Figure 2.3: STM images of platinum trimers on graphite, (a) - (c), and schematic drawings of their structure, (d) - (f).
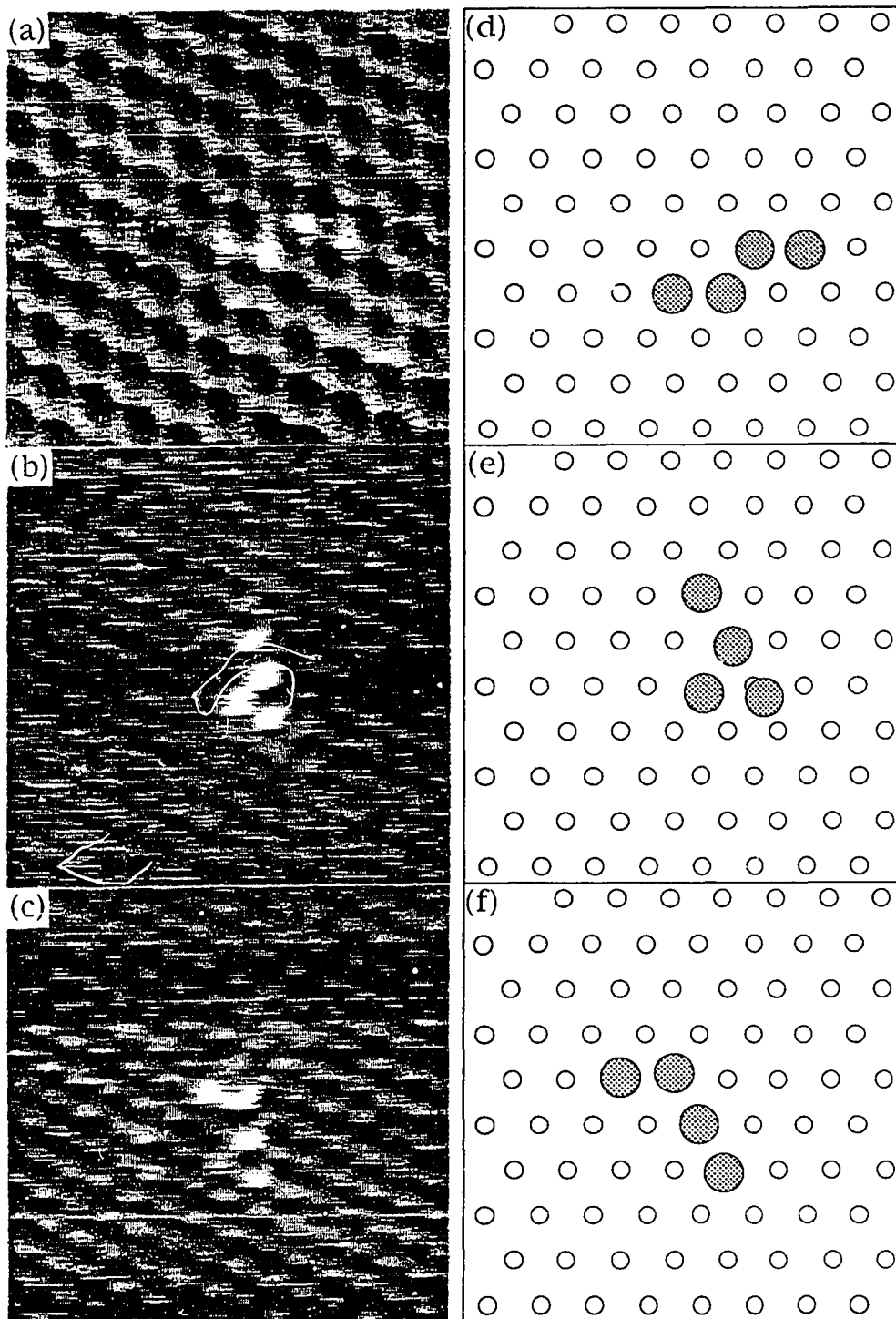
Figure 2.4: STM images of platinum tetramers on graphite, (a) - (c), and schematic drawings of their structure, (d) - (f).
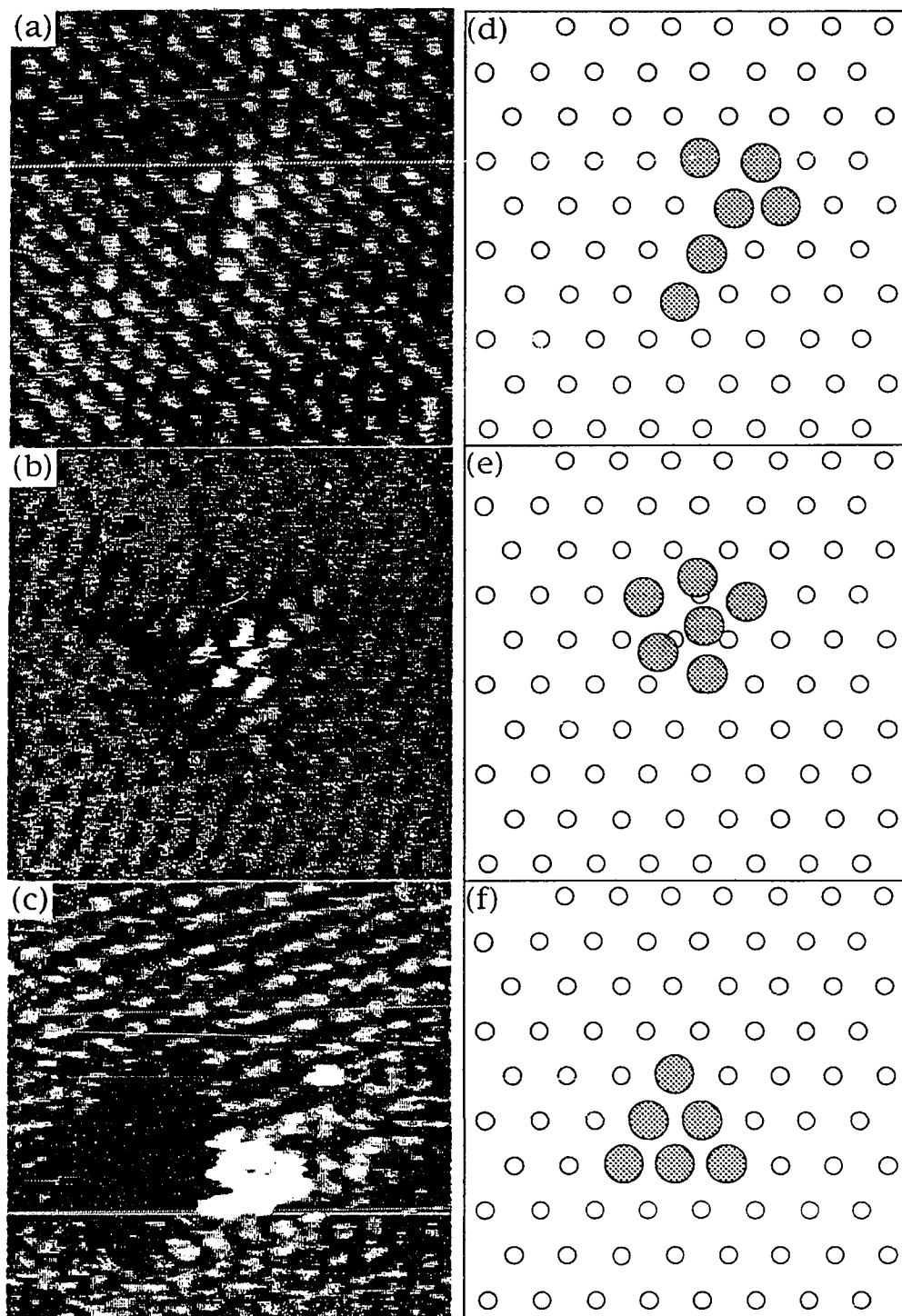
Figure 2.5: STM images of platinum hexamers on graphite, (a) - (c), and schematic drawings of their structure, (d) - (f).
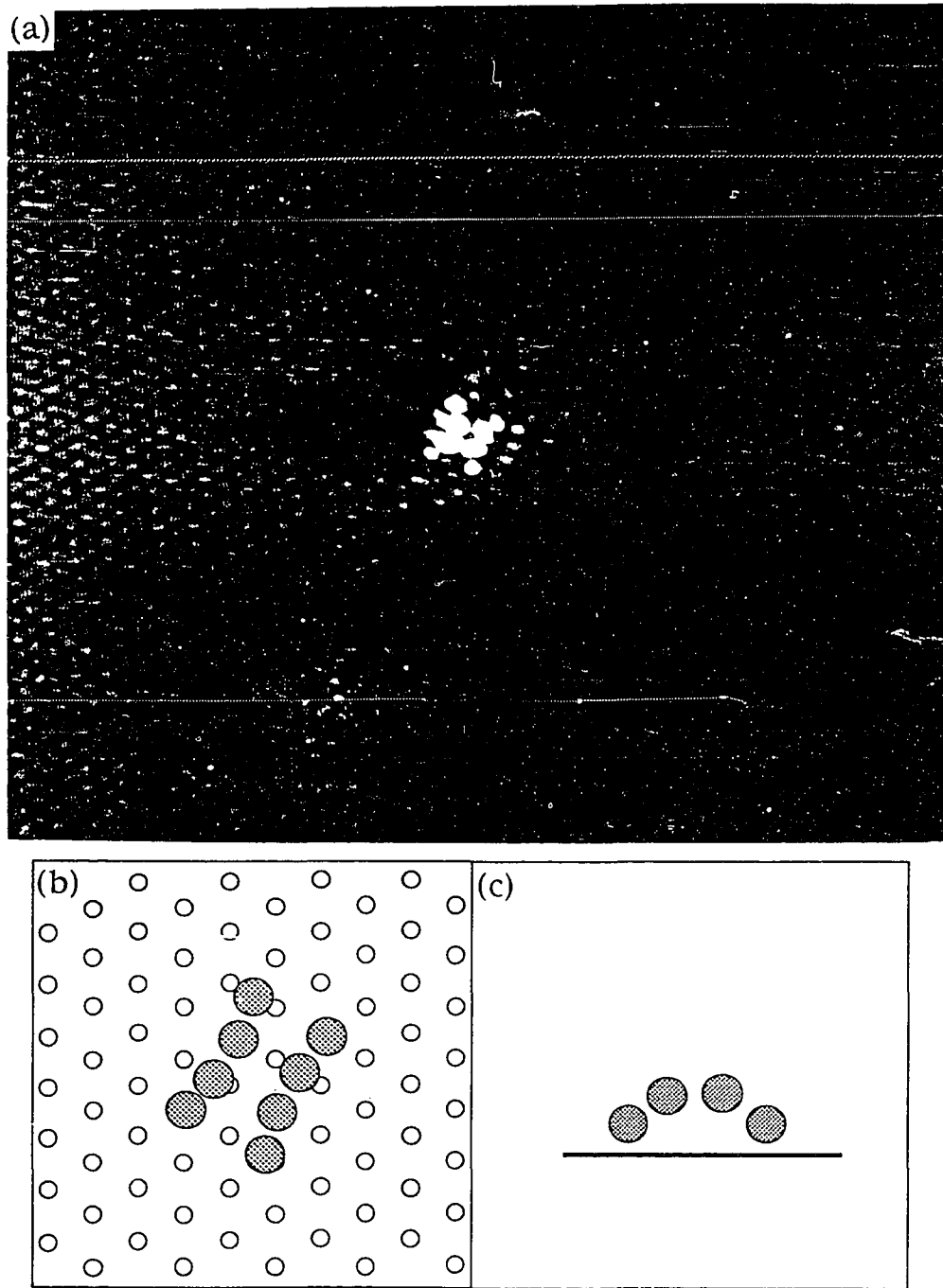
Figure 2.6: (a) STM image of a platinum octamer on the surface of graphite. (b) Schematic drawing of the platinum octamer. (c) Side view of the platinum octamer.
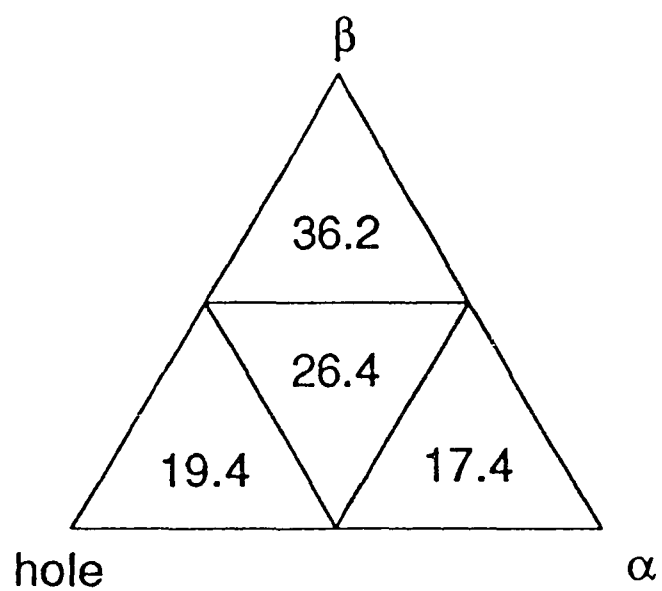
Figure 2.7:   Adsorption site distribution for platinum atoms on graphite.

bond length distributions
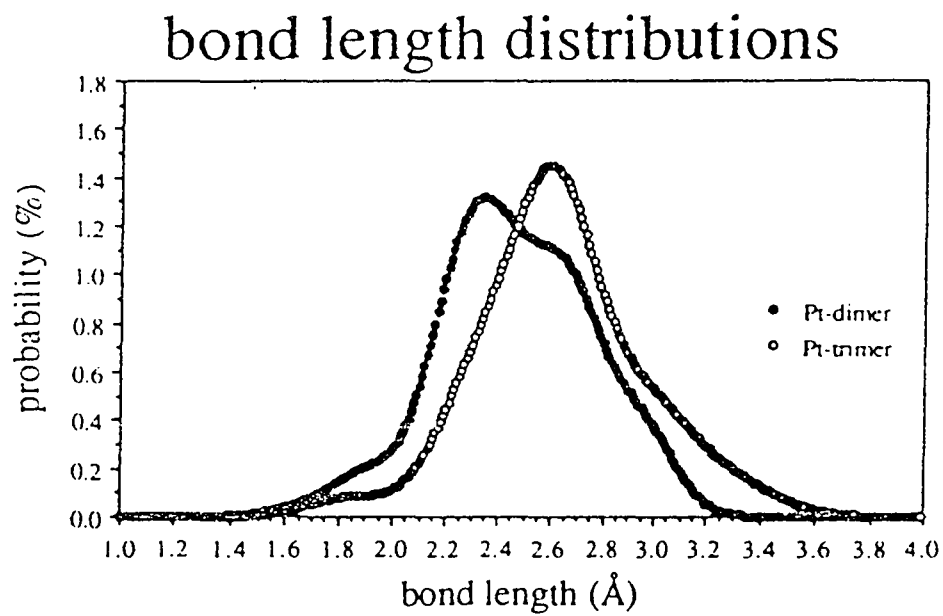
Figure 2.8: Bond Length distributions for platinum dimers and trimers on graphite.

Chapter III

**PERIODIC CHARGE-DENSITY MODULATIONS
ON GRAPHITE NEAR ADSORBED CLUSTERS**

3.1   Introduction

Recently superstructures on graphite near defects have been reported.[1-5] The defects can be steps, holes in the graphite lattice or adsorbed molecules. The superstructures have been found to have a periodicity of $(\sqrt{3}\times\sqrt{3})R30°$ and decay over a distance of a few nanometers. Mizes and Foster[4] have proposed an electronic perturbation model for such structures near isolated adsorbed molecules. They suggest that the adsorbed molecules perturb the charge density along the surface of graphite giving periodic oscillations similar to Friedel oscillations. The oscillations have a periodicity $\sqrt{3}$ times the graphite lattice constant, and the symmetry of the oscillations reflects the nature of the defect. Nakagawa et al.[5] have observed similar structures near a step. Besides the $(\sqrt{3}\times\sqrt{3})R30°$ periodicity, they find that in a unit cell of the $\sqrt{3}\times\sqrt{3}$ structure the three β-site atoms show different brightness. Close to the step they observe an apparent horizontal displacement of graphite atoms and a so called "triplet" structure. They ascribe the observed features to an interference of electron waves scattered at the step. It successfully explained the $(\sqrt{3}\times\sqrt{3})R30°$ periodicity, the brightness difference and the decay with distance but could not explain the apparent horizontal displacement of the graphite atoms and the "triplet" structure.

Although various STM images of clean graphite have been reported,[6] the superstructures which have a periodicity of $(\sqrt{3}\times\sqrt{3})R30°$ are completely different and are found only near defects on graphite. This suggests that they are induced by a perturbation caused by surface defects. However, it is still unclear how the defects influence the nearby graphite lattice. The electronic perturbation model by Mizes and Foster[4] and the electron wave interference model by Nakagawa et al.[5] explain only some of the features. To fully understand the physics of these superstructures one needs more experimental data and more theoretical analyses.

In this chapter we show a variety of superstructures of graphite found near adsorbed clusters, namely, platinum and cobalt clusters. We show that the observed features are mainly due to an electronic effect which can be described by a superposition of the graphite lattice and a periodic modulation of the surface charge density localized in the surrounding regions of the adsorbed clusters. The effects of such modulations on the cluster structure will also be discussed.

3.2   Experiment

The experiments were performed at room temperature using a scanning tunneling microscope[7] in air. All the images presented here were taken in constant current mode where the tip-sample distance was kept constant and the variation of the z-motion of the tip was recorded.

The platinum samples were the same samples used in the discussion in Chapter II. The cobalt samples were prepared in a high vacuum (10^{-7} Torr) chamber by vapor deposition of cobalt on freshly cleaved graphite substrates. After evaporation, the samples were kept in the

vacuum chamber overnight to allow slow oxidization before exposition to air. This process has been found to be critical in forming stable and conducting cobalt particles on the graphite surface. Evidence of metallic cobalt was seen in XPS spectra for cluster size greater than 4 nm.[8] Analysis by XPS also showed a typical ~5% coverage of a cobalt monolayer on the graphite surface.

The sample was then transferred to a STM operating at atmospheric conditions. The STM images were taken at constant current mode with positive tip bias-voltages of 3 - 160 mV and tunneling currents of 1.5 - 14.0 nA. At large scales (100 - 440 nm) we imaged platinum clusters of sizes 0.8 - 2.5 nm randomly distributed on the graphite surface. The average size of cobalt clusters was found slightly larger than platinum clusters, ranging from 1.0 - 6.0 nm. We have investigated five platinum samples and two cobalt samples and various superstructures near clusters on graphite have been found on all of the samples.

3.3   Results and Discussion

3.3.1 Superstructures on Graphite Near Platinum Clusters

All the images shown in this chapter were reproducible for at least five scans (about 30 seconds). Occasionally the structures changed from one type to another during the process of imaging and in some cases disappeared after a period of time.

Figure 3.1 shows a typical grey-scale image of a small platinum cluster adsorbed on graphite. It appears as the bright area in the center and has a size of about 0.8 nm. Around the cluster the graphite lattice appears to be distorted to form different superstructures as shown at the

upper left (A), right (B) and lower left (C) of the cluster. The intensity of the superstructures decays away from the cluster over a distance of 2 - 3 nm. Similar images of superstructures were obtained quite often near different platinum clusters.

In Figure 3.2 - Figure 3.11 we show ten different superstructures found near different clusters, where (a) is the STM topview image and (b) is the corresponding schematic model. In (b) the hollow circles represent the positions of the carbon atoms in the undisturbed triangular or hexagonal graphite lattice.[9] The solid circles show the positions of the bright spots in the STM images. For each of the images we performed a two-dimensional Fourier analysis. The first-order Fourier components which correspond to the superstructures are indicated as dashed lines in (b). From the Fourier analysis we can divide the superstructures into three categories, each contains one, two or three dominant Fourier components.

Figure 3.2 shows a superstructure where one of the Fourier components is dominant and is oriented at an angle of 30° to the graphite lattice. The period of the Fourier components is 1.5a, where a = 0.245 nm is the lattice constant of the graphite. Figure 3.3 - Figure 3.6 show four superstructures where two of the Fourier components are dominant. Their directions have an angle of 60° relative to each other and 30° to the graphite lattice. The period of the Fourier components is again 1.5a. Figure 3.7 - Figure 3.10 show another four superstructures. Their Fourier components reveal the same features in periodicity and orientation as the previous ones except that all three Fourier components are comparable and each has an angle of 60° to the other. Also for all the superstructures which we have analyzed, each Fourier component has a phase relative to the graphite lattice and these phases are independent from each other.

34

Figure 3.11 shows a special superstructure where one of the two dominant Fourier components has a period of 0.75a, which is half of the period of the other Fourier components. But its orientation is still 30° rotated relative to the graphite lattice.

3.3.2 Superstructures on Graphite Near Cobalt Clusters

For our cobalt samples, superstructures of graphite were also imaged near small (1 - 3 nm) cobalt clusters. Although most of them are of the same types as those observed near platinum clusters, new types of superstructures were found.

In Figure 3.12 - 3.16 we show five additional structures on graphite near cobalt clusters, where (a) is the STM image and (b) is the corresponding schematic model. Similar to those found near platinum clusters, the superstructures contain Fourier components with a period of 1.5a and rotated 30° relative to the graphite lattice. The superstructures in Figure 3.12 and 3.13 contain only one dominant Fourier component, while in Figure 3.14, 3.15 and 3.16, they contain all three Fourier components.

The presence of superstructures near cobalt clusters as well indicates that chemical identity of the clusters is irrelevant to the observed features. For other metal clusters such as silver and gold adsorbed on graphite, similar superstructures have also been observed previously both in air and in ultra-high vacuum.[10]

3.3.3 Periodic Charge-density Modulations (PCDM) on Graphite

The fifteen superstructures shown in Figure 3.2 - 3.16, although different in appearance, have many characteristics in common. They are localized in small areas near adsorbed clusters and decay within a distance

of 2 - 5 nm into the graphite lattice. The Fourier components of these structures always have a period of 1.5a (except in one case 0.75a) and their orientation is rotated by 30° with respect to the graphite lattice.

We exclude the possibility that the superstructures are due to multiple tip effects because: (i) the superstructures have been found only near the platinum particles but never on plain graphite, (ii) different superstructures have been imaged using the same tip and even within the same scan lines, as seen in Figure 3.1 where regions A and B are scanned alternatively from right to left.

We also exclude the possibility that the superstructures are merely due to an atomic reconstruction of the graphite lattice. Figure 3.17(a) shows a STM image of a superstructure analogous to the one in Figure 3.2(a). Figure 3.17(b) shows a section taken along the line AB as indicated in Figure 3.17(a). Going from right to left the section curve shows first the atomic corrugation of the graphite atoms at β-sites and then the corrugation of the superstructure. The arrow indicates the position where the peaks of two graphite atoms begin to grow together and become one peak. From there on every other peak is actually positioned over two graphite atoms as indicated by the solid circles. Since the two carbon atoms can not be that close, the bright spots which form the superlattice do not represent the real positions of the graphite atoms. Therefore the observed superstructures are not a real picture of a possible surface atomic reconstruction of the graphite lattice, but are due to a periodic modulation of the surface charge density.

To further understand the physics of the superstructures one has to take into account all the detailed features of the observed structures. We ascribe these structures to a superposition of the graphite lattice and a

3 6

localized periodic charge-density modulation (PCDM). This model explains all the features we have observed. As shown in Figure 3.2 -3.16 (b), the dashed lines which were used to represent the Fourier components of the superstructures can now be used to represent the maxima of the PCDM. They have a period of 1.5a and are oriented in the three symmetry directions, each rotated 30° to the graphite lattice.

Due to the periodic charge-density modulation the underlying graphite atoms appear to be either highlighted if the maxima sit right on the atoms or otherwise shifted toward the maxima. For example, the superstructure in Figure 3.2 is formed by the modulation in only one direction. Therefore the graphite atoms appear to form a line-pattern structure. Similar arguments are also applicable to the superstructures in Figure 3.3 - 3.11 where the periodic charge-density modulations exist in two or three directions.

The five additional superstructures found near cobalt clusters can also be explained in terms of the PCDM model. The structures in Figure 3.12 and 3.13 are formed by superimposing a PCDM component on the graphite triangular and honeycomb lattice, respectively. In Figure 3.14, the superstructure shows a large honeycomb pattern similar to that of Figure 3.8. It is modulated by three sets of PCDM components with graphite showing a honeycomb lattice. Also, the superstructure in Figure 3.15 is similar to that of Figure 3.9 except that the graphite shows a honeycomb lattice in Figure 3.15.

A more complicated structure combining two superstructures is displayed in Figure 3.16. A large triangular lattice is formed from the bright spots at the bonds between an α-site and a neighboring β-site. In between are less bright chains of connected hexagons. With the PCDM

model, this structure can be produced by superimposing three sets of PCDM components on the honeycomb graphite lattice. As illustrated in (b), two sets of the PCDMs have their vertices on the highlighted bonds forming the large triangular lattice. The third set of the PCDMs shown as horizontal dashed lines has a smaller intensity and therefore highlights the less bright hexagon chains.

Therefore, the fifteen different superstructures are formed by the combination of the underlying graphite lattice, either triangular or hexagonal, and the PCDMs with up to three sets of components. The three PCDM components act rather independently and can have different intensities and different phases relative to graphite lattice.

The difference in the intensities of the PCDM components sometimes gives rise to small apparent rotations of the unit cells of the superstructure. Figure 3.18 (a) shows a STM image where the superstructure is similar to that of Figure 3.3. It is formed by two PCDMs with their vertices sitting on the bridge sites of the graphite lattice. Therefore the atoms next to the vertices are highlighted and appear as dimers. Along the line indicated in Figure 3.18 (a) the orientation of the dimers gradually changes from the lower part to the upper part of the image. At the lower part of the image the dimers are aligned along the graphite orientation. But when going to the upper part the dimers rotate gradually relative to the graphite lattice up to a maximum rotation of 15°. This gradual dimer rotation can be explained by the different intensities and different decay rates of the PCDMs in the two directions. As shown in Fig.18 (b), when the modulation in one direction is stronger than in the other the position of the atoms seems to be shifted toward the stronger modulation so that the dimers appear to be rotated. This rotation also decays gradually with the distance from the particle.

In Figure 3.8(a) the superstructure shows a regular brightness difference of the white spots in a unit cell of the superlattice. The same "brightness difference" was also observed by Nakagawa et al..[5] With our PCDM model it can be easily produced by a small phase shift of the modulation in all three directions as shown in the inset of Fig.8 (b). Therefore, in a hexagon of the superlattice, three of the outer atoms are highlighted most, the other three are highlighted less but are still more highlighted than the center atom.

Because of the many possibilities of superimposing the underlying graphite lattice with the PCDMs of various intensities and phases, we expect to see more types of superstructures in the future.

Although the PCDM model explains almost all the observed features, it is still a phenomenological description. The physical origin of the PCDMs is not well understood. It may be explained in the framework of charge-density waves (CDW) in conjunction with periodic lattice distortions (PLD), phenomena observed for various quasi-two-dimensional layered materials. CDW's are caused by the instability of the Fermi surface and have been studied by STM for transition metal dichalcogenides.[11] Recently, various CDW vertex structures were found for $TaSe_2$, and could be explained by a phase-shift procedure,[12] similar to the one used in this work. It involves different lock-in positions for periodic charge-density lattices relative to the underlying atomic lattice. However, such metastability of a CDW, as well as its periodicity and orientation, has not yet been explained theoretically.

Surface stress may be another possible explanation. The stress exerted by the adsorbed clusters may induce a distortion of the Fermi surface and, as a consequence, a charge-density redistribution. Also, the

occasional changes in the superstructures may be due to slight variations in the bond lengths and orientations of the atoms in the clusters,[13] which could affect the strain on the substrate and lead to different surface electronic arrangements.

The period of 1.5a, as well as the rotation of 30°, corresponds to the second-nearest neighbor of the graphite lattice of β-sites. For a monolayer of graphite, the corresponding Brillouin zone is a regular hexagon and the Fermi surface collapses to points at the corners of the Brillouin zone.[14] In a tight-binding calculation performed by Mizes and Foster,[4] two wave functions concentrated on β atoms were expressed as a symmetric and antisymmetric linear combination of the wave vectors oriented toward the corners of the hexagonal Brillouin zone. The magnitude and orientation of these wave vectors give rise to a wavelength of 1.5a and a rotation of 30° relative to the graphite lattice. This may explain the preferred periodicity and orientation of the PCDM. In addition, it also indicates that the PCDM is related to the graphite itself and is induced by the defects on the graphite surface.

3.3.4 PCDM Feedback on Atomic Structures of Clusters

The cluster-induced superstructures may have a decisive effect on the atomic arrangements in the clusters. For example, in Figure 3.17, the platinum clusters has induced a PCDM yielding a periodic line pattern rotated 30° with respect to the graphite lattice. Then, as a response, the atoms in the cluster moved to adsorption sites with maximum PCDM intensity and form a rectangular net. Such effects of the PCDMs on the structure of clusters are not significant for large particles. Small clusters, however, have a tendency to arrange themselves accordingly to the maxima

of the PCDMs. As another example, the dimer in the lower left corner of Figure 3.16 is oriented along one the PCDM directions.

3.4   Conclusions

We have imaged fifteen different superstructures on highly-oriented pyrolytic graphite near adsorbed clusters using a scanning tunneling microscope. Independent of the chemical identity of the clusters, these superstructures were found in small areas near the clusters and decayed within a distance of 2 - 5 nm into the graphite lattice. They can be explained by the superposition of the periodic charge-density modulations with the graphite atomic lattice. The PCDMs are localized in small areas near adsorbed clusters, or generally near defects, on graphite and decay with distance from the clusters. They have a period of 1.5a and exist in three possible directions, each rotated 30° relative to the graphite lattice. The overall image of the superstructures depends on the dominant PCDMs and their intensities and phases relative to graphite atomic lattice.

The PCDMs induced by adsorbed clusters may have a decisive effect on the atomic arrangements in the clusters. Atoms in clusters tend to bind to the sites with maximum intensity of the modulation.

3.5   References

1.   Physics Today **41**, 129 (1988).

2.   T. R. Albrecht, H. A. Mizes, J. Nogami, S.-I. Park, and C. F. Quate, Appl. Phys. Lett. **52**, 362 (1988).

3. J. P. Rabe, M. Sano, D. Batchelder, and A. A. Kalatchev, Journal of Microscopy **152**, 573 (1988).

4. H. A. Mizes and J. S. Foster, Science **244**. 559 (1989).

5. Y. Nakagawa, H. Bando, M. Ono, and K, Kajimura, "$\sqrt{3}\times\sqrt{3}$ Structure on Graphite Surface," unpublished.

6. H. A. Mizes, S.-I. Park, and W. A. Harrison, Phys. Rew. B **36**, 4491 (1987).

7. Digital Instruments, Inc., Santa Barbara, CA, USA.

8. A. Rizzetti, J. Xhie, K. Sattler, D. Yamamoto, and W. Pong, J. of Electron Spectrosc. Relat. Phenom. **58**, 359 (1992).

9. D. Tomanek, S. Louie, H. J. Mamin, D. W. Abraham, R. E. Thomson, E. Ganz, and J. Clarke, Phys. Rev. B **35**, 7790 (1987).

10. E. Ganz, K. Sattler, and J. Clarke, unpublished results.

11. R. V. Coleman, B. Giambattista, P. K. Hansma, A. Johnson, W. W. McNairy, and C. G. Slough, Adv. Phys. **37**, 559 (1988).

12. G. Raina, K. Sattler, U. Müller, N. Venkateswaran and J. Xhie, J. Vac. Sci. Technol. B 9 (2), 1039 (1991).

13. E. Ganz, K. Sattler, and J. Clarke, Phys. Rew. Lett. **60**, 1856 (1988).

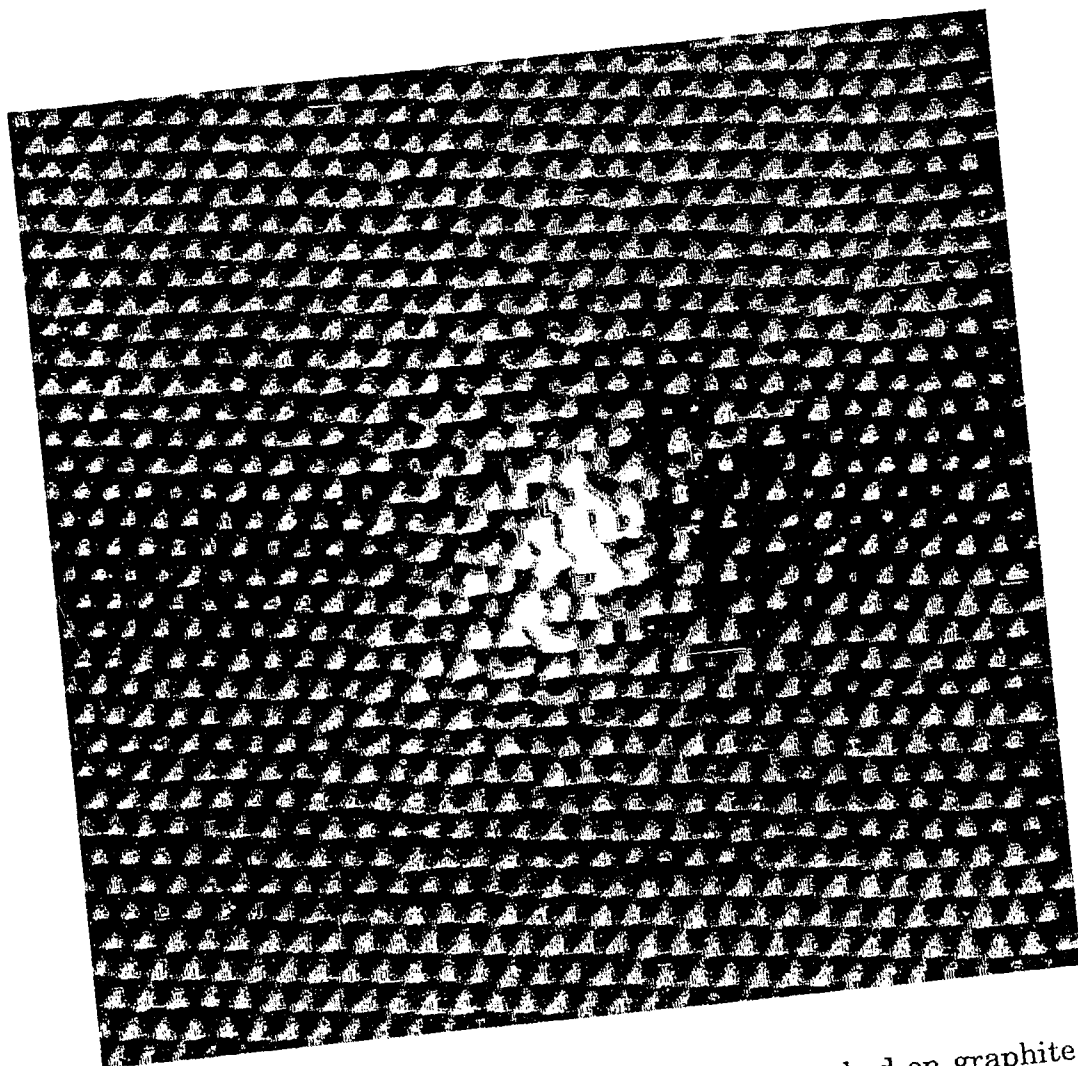14. J. Tersoff, Phys. Rev. Lett. **57**, 440 (1986).

Figure 3.1: STM image of a platinum particle adsorbed on graphite. The particle appears as the bright area in the center and has a size of about 0.8 nm. Around the particle there are regions of graphite forming superstructures as indicated by A, B, C.
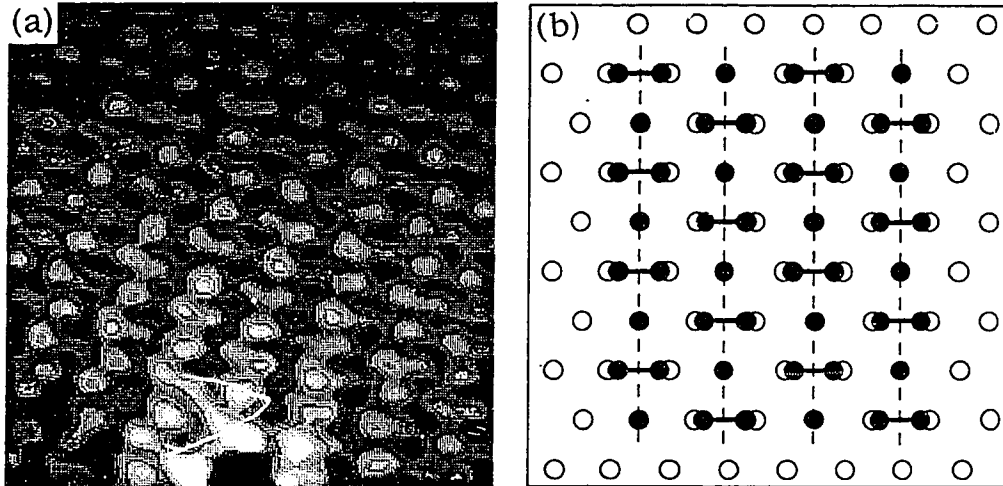
Figure 3.2:   (a) STM image of a superstructure with one dominant set of the PCDMs superimposed on the hexagonal graphite lattice. (b) Corresponding schematic model.
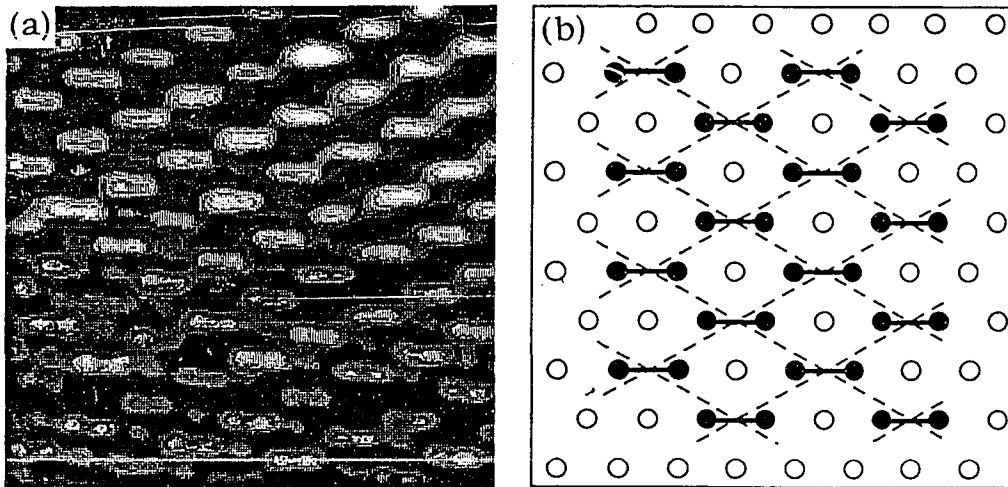

Figure 3.3:   (a) STM image of a superstructure with two dominant sets of the PCDMs superimposed on the hexagonal graphite lattice. (b) Schematic model.

Figure 3.4:   (a) STM image of a superstructure with two dominant sets of
the PCDMs superimposed on the hexagonal graphite lattice.
(b) Schematic model.

Figure 3.5:   (a) STM image of a superstructure with two dominant sets of
the PCDMs superimposed on the honeycomb graphite lattice.
(b) Schematic model.

Figure 3.6:   (a) STM image of a superstructure with two dominant sets of the PCDMs superimposed on the honeycomb graphite lattice. (b) Schematic model.
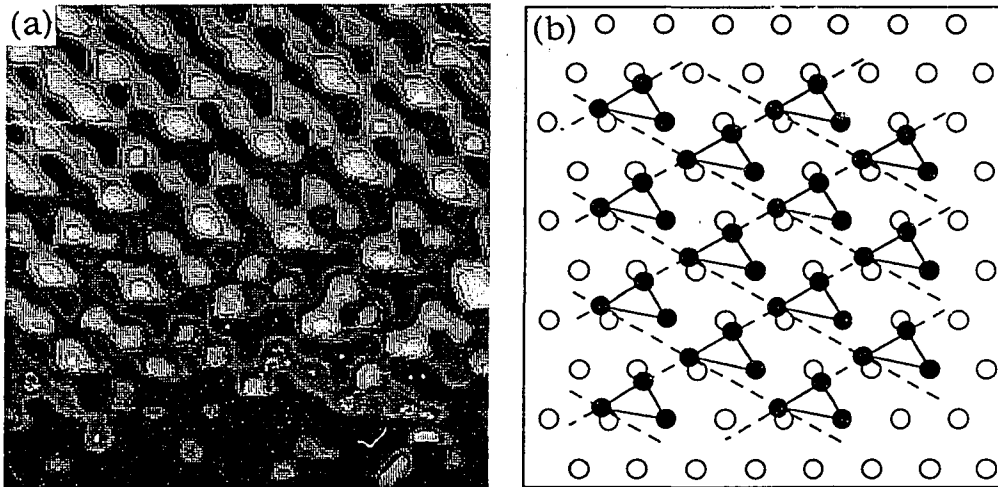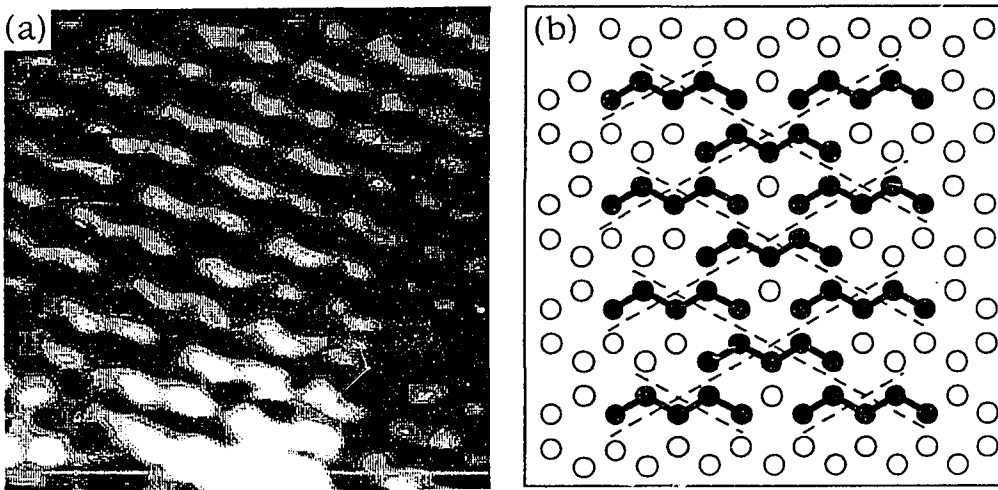

Figure 3.7:   (a) STM image of a superstructure with three dominant sets of the PCDMs superimposed on the hexagonal graphite lattice. (b) Schematic model.

Figure 3.8:   (a) STM image of a superstructure with three dominant sets of the PCDMs superimposed on the hexagonal graphite lattice. (b) Schematic model. The inset shows the model of the brightness difference observed in (a).

Figure 3.9:   (a) STM image of a superstructure with three dominant sets of the PCDMs superimposed on the hexagonal graphite lattice. (b) Schematic model.
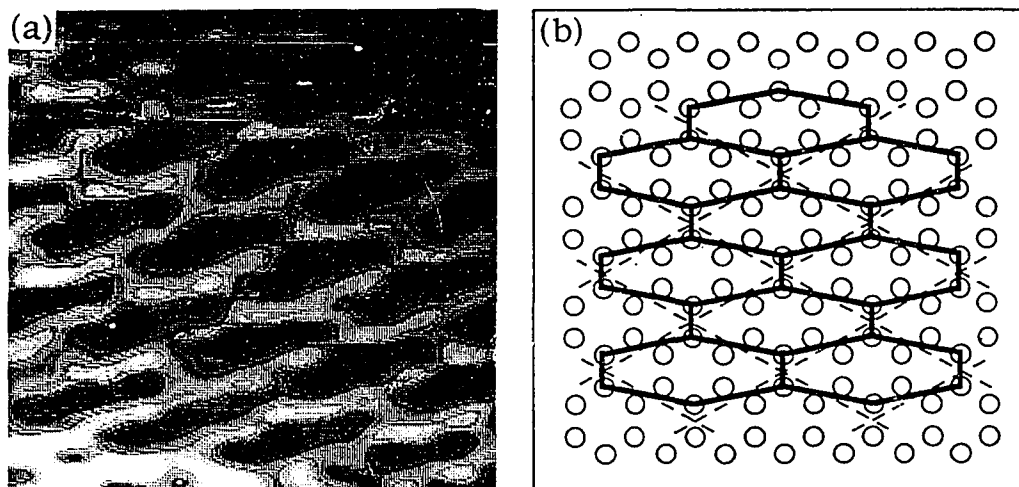
Figure 3.10: (a) STM image of a superstructure with three dominant sets of the PCDMs superimposed on the honeycomb graphite lattice. (b) Schematic model.

Figure 3.11: (a) STM image of a superstructure with two dominant sets of the PCDMs superimposed on the hexagonal graphite lattice. One of the sets has a period of 0.75a. (b) Schematic model.
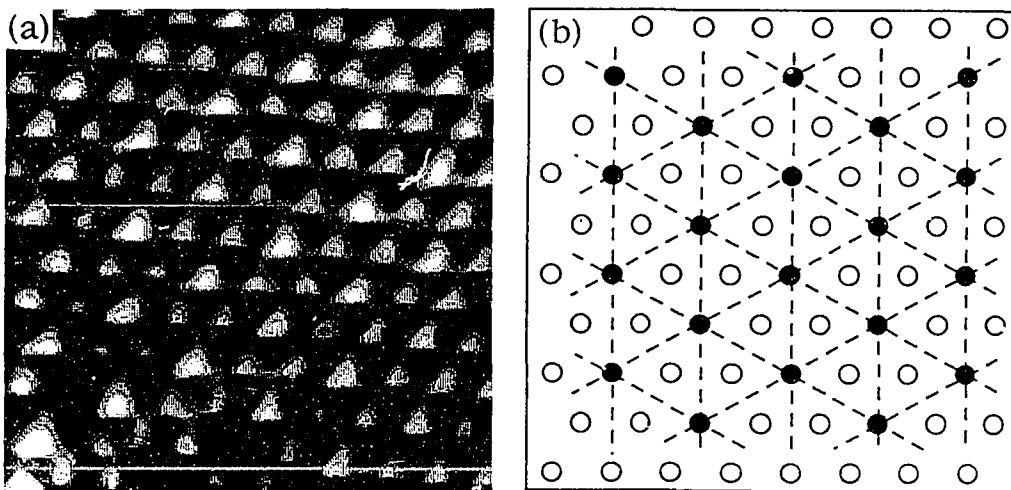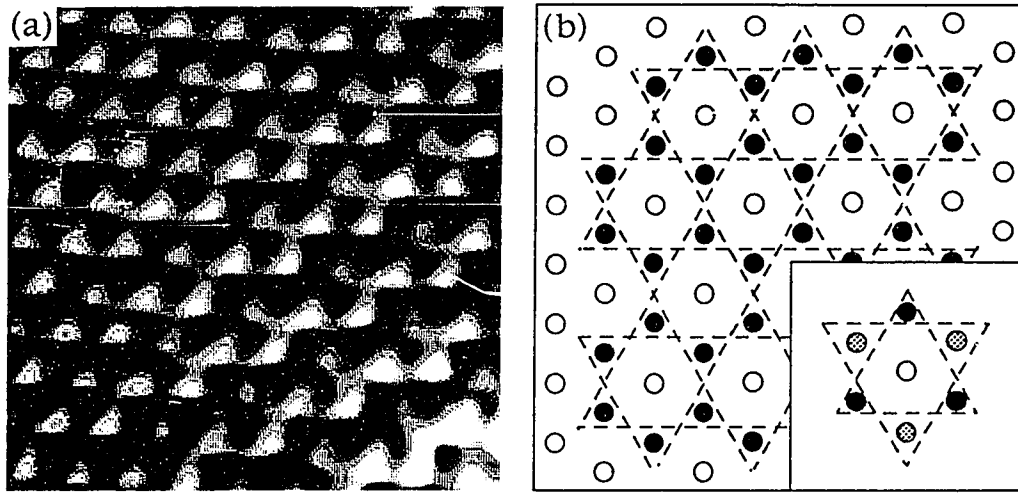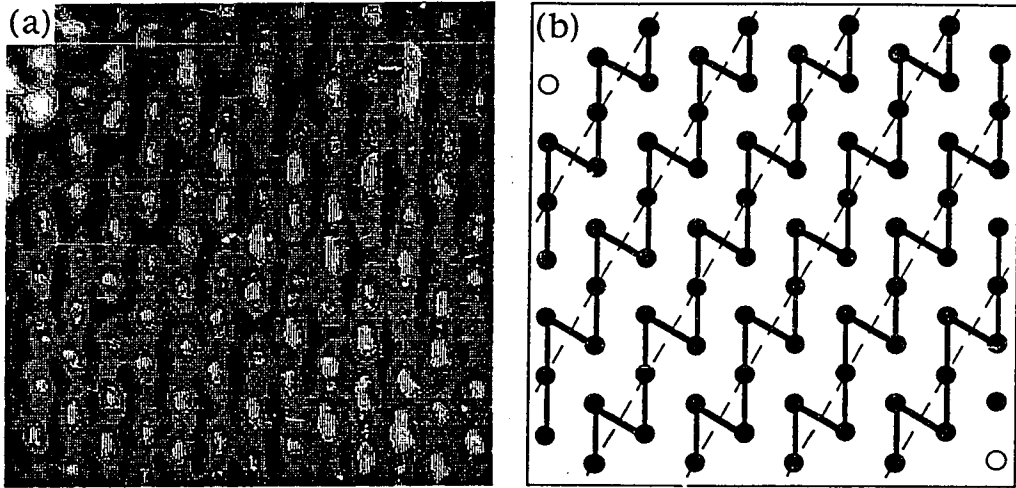
Figure 3.12: (a) STM image of a superstructure with one dominant set of the PCDMs superimposed on the hexagonal graphite lattice. (b) Schematic model.
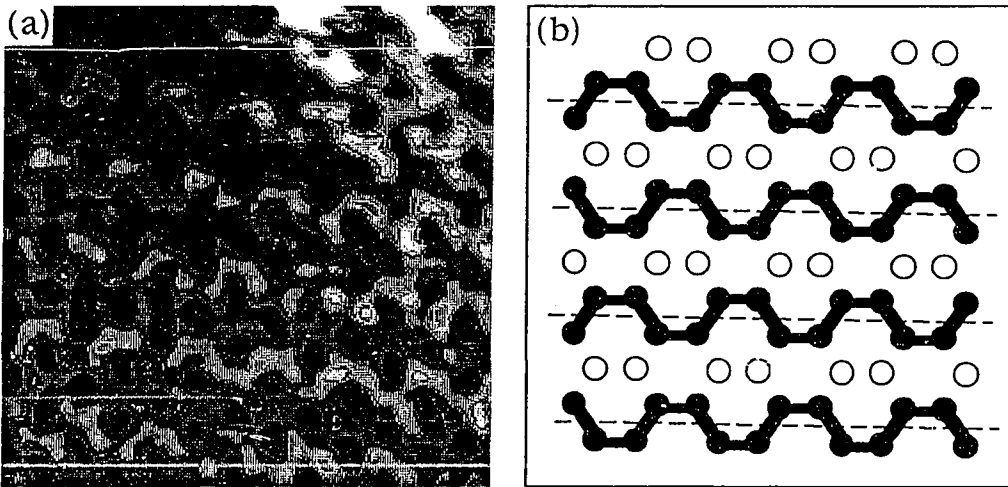
Figure 3.13: (a) STM image of a superstructure with one dominant set of the PCDMs superimposed on the honeycomb graphite lattice. (b) Schematic model.
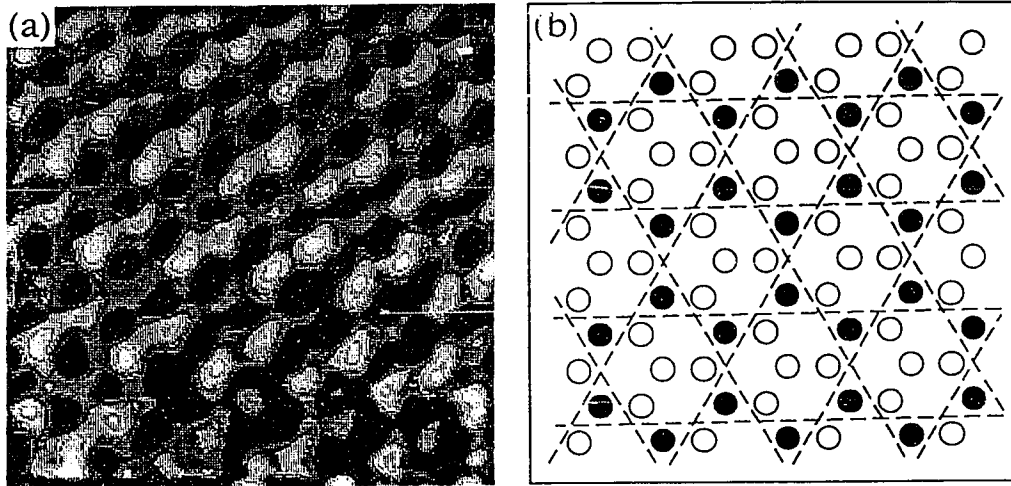
Figure 3.14: (a) STM image of a superstructure with three dominant sets of the PCDMs superimposed on the honeycomb graphite lattice. (b) Schematic model.
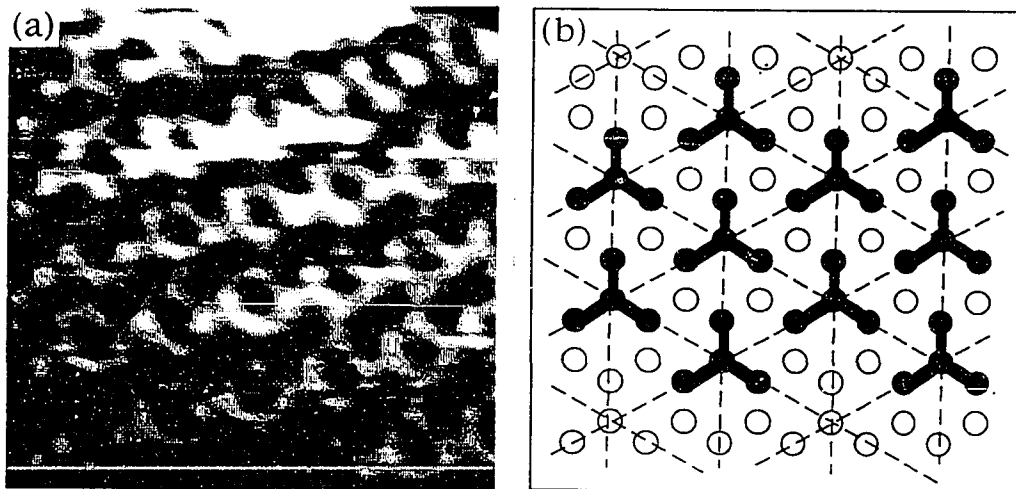
Figure 3.15: (a) STM image of a superstructure with three dominant sets of the PCDMs superimposed on the honeycomb graphite lattice. (b) Schematic model.
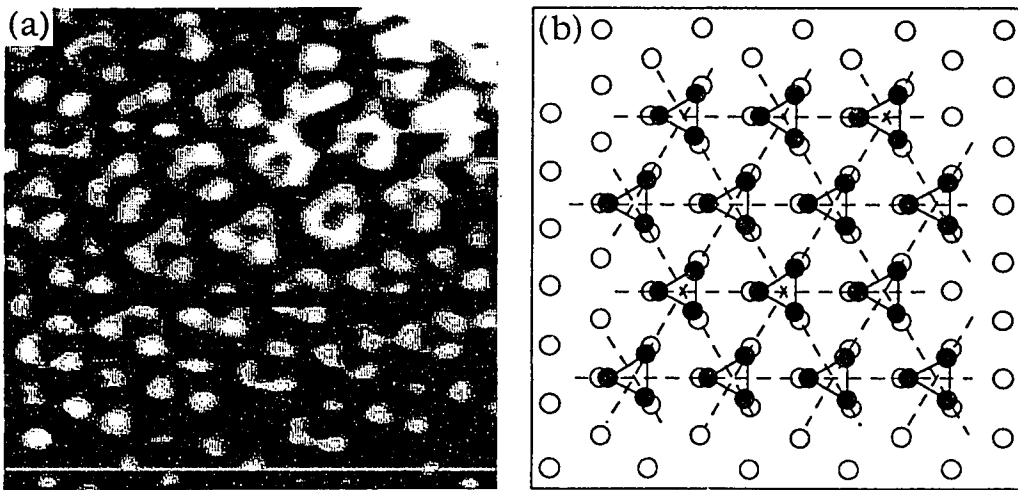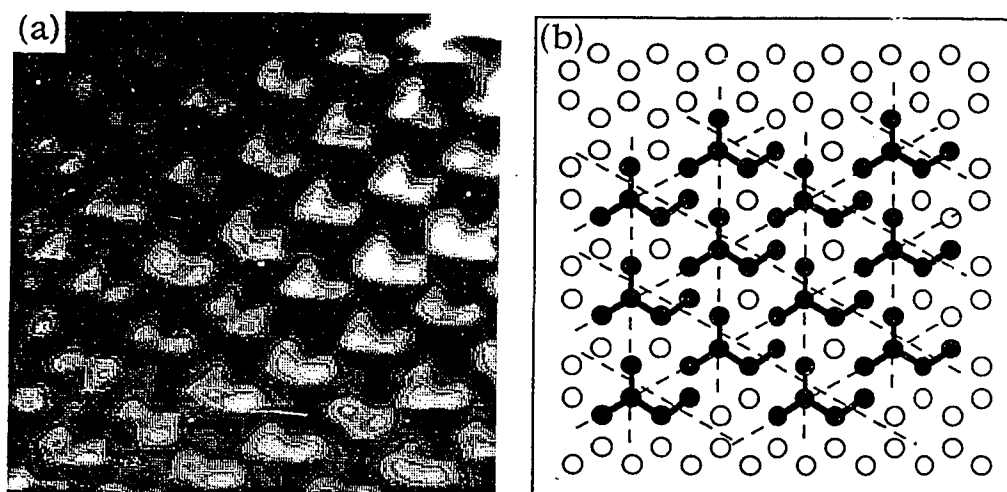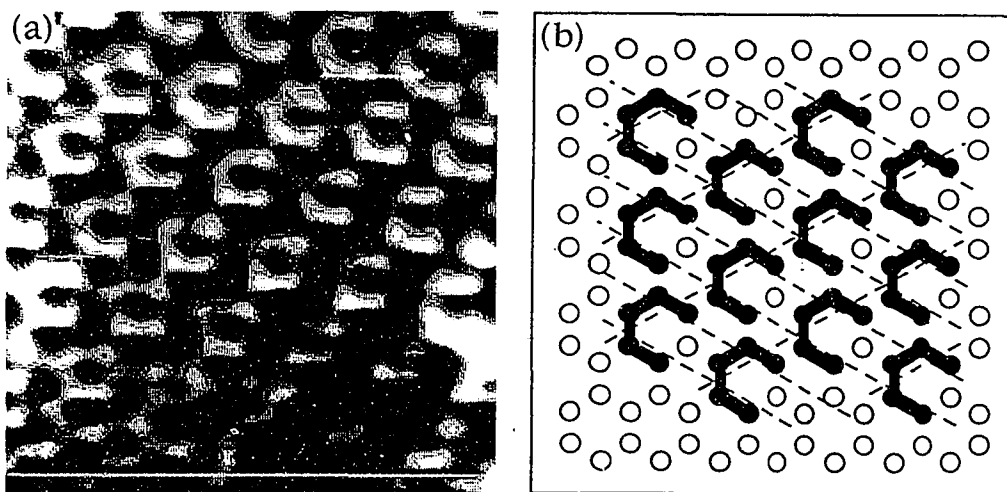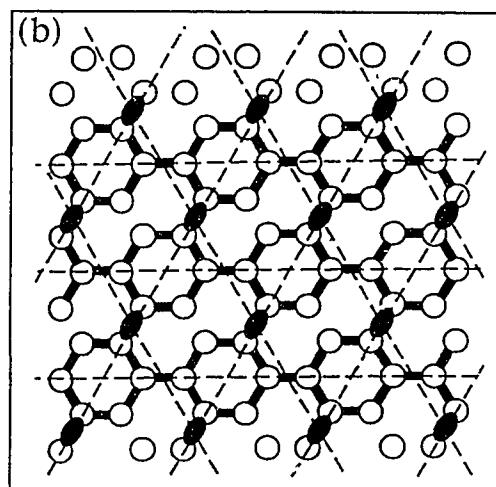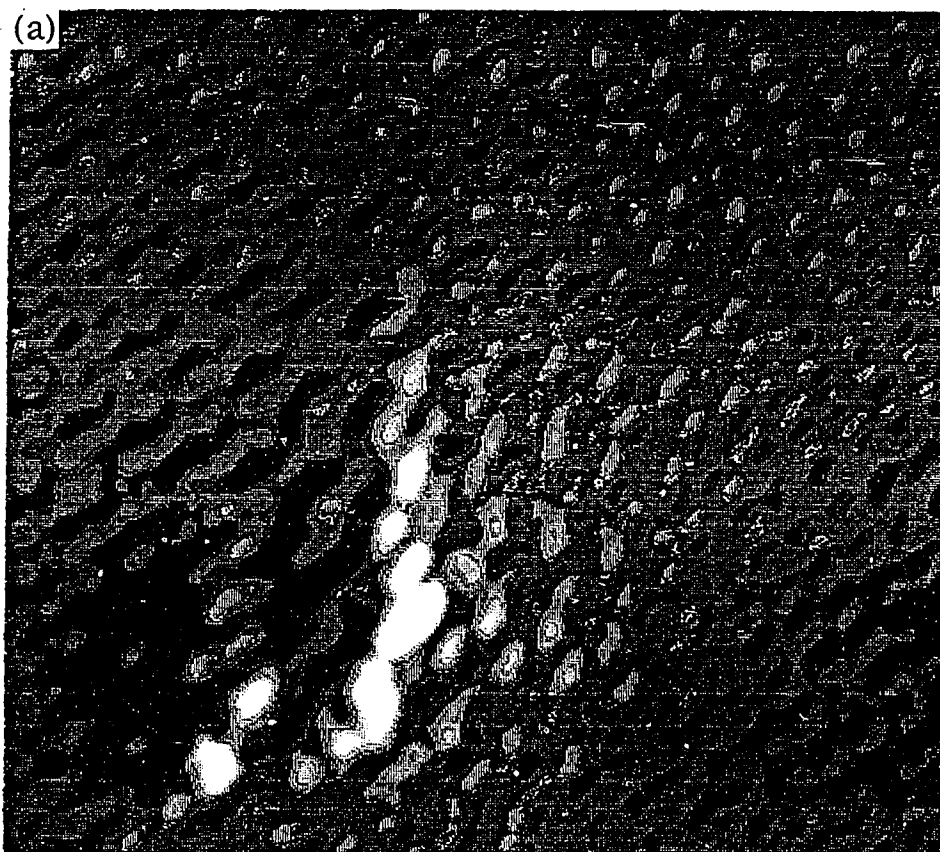
Figure 3.16: (a) STM image of a superstructure with three dominant sets of the PCDMs superimposed on the honeycomb graphite lattice. (b) Schematic model.
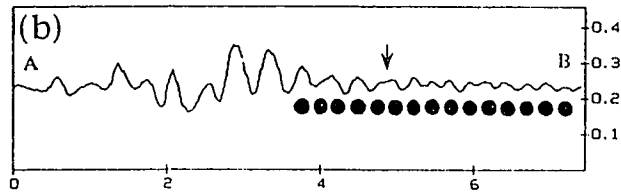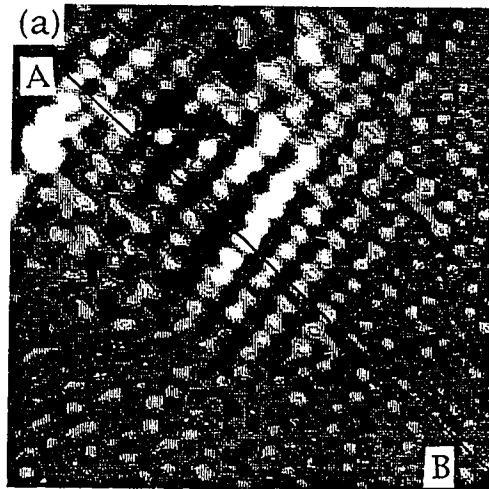
Figure 3.17: (a) STM image of a superstructure similar to that in Fig. 2. (b) A section taken along the line AB as indicated in (a). The solid circles represent the positions of the graphite β atoms. The arrow indicates the position where the peaks of two graphite atoms begin to grow together.
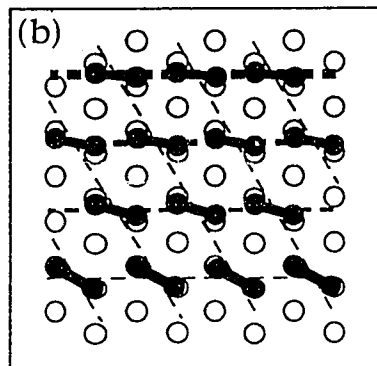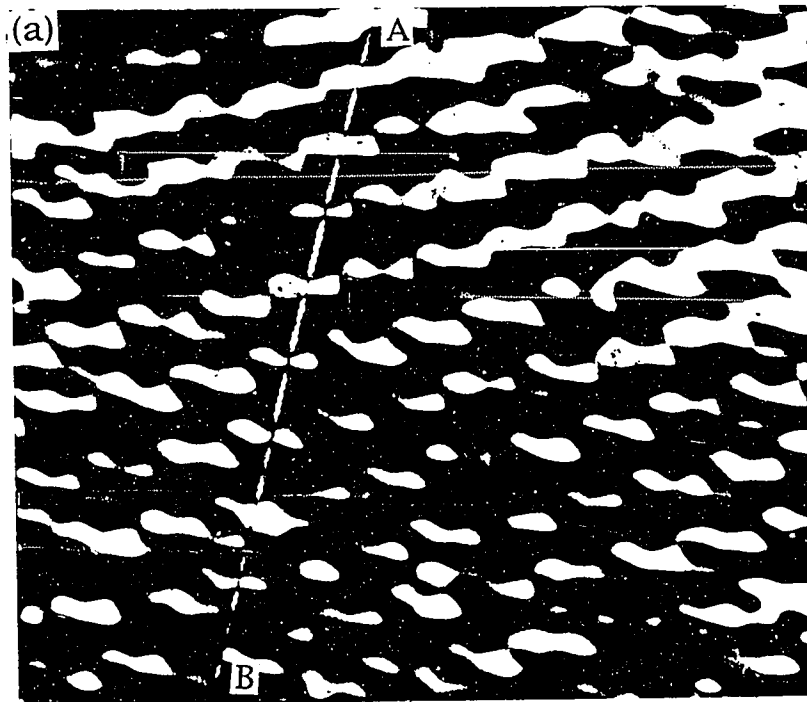
Figure 3.18: (a) STM image of a superstructure similar to that in Fig. 3. The orientation of the dimers along the line changes gradually from bottom to top. (b) Schematic model of the superstructure in (a) showing the gradual rotation of the dimers. The dashed lines represent the maxima of the PCDM's and their thickness is proportional to the intensity of the PCDMs.

Chapter IV

GIANT LATTICES ON GRAPHITE

4.1   Introduction

As a popular substrate, graphite has been imaged extensively using the scanning tunneling microscope. STM images of graphite often reveal unusual features such as large atomic corrugation,[1,2] asymmetry in the apparent heights of neighboring carbon sites,[3] and superstructures near defects as discussed in the last chapter.[4] More recently, anomalous large-scale periodic patterns have been observed on graphite in addition to its atomic structure.[5-10] They had hexagonal symmetry with periodicities up to 44 nm and occurred in regions with observable boundaries. Kuwabara et al.[5] suggested that these superperiodicities may be rotational Moire patterns resulting from the overlap between a misoriented top layer of graphite and the underlying graphite single crystal. Since the STM can only image the top layer, the relative rotation of this layer to the underlying graphite can not be directly shown in the STM images. Therefore the suggestion of Moire patterns remained a speculation.

In this chapter we report similar superperiodic patterns, which we call "giant lattices," observed from four separate graphite samples. On one of the samples we have observed, for the first time, a misorientation of graphite which results in the observed giant lattice. We also show that, although the STM can only see the top layer, the effects from deeper layers on a rotated top layer can lead to giant lattices in the STM images. We

develop a complete description to account for the detailed features of giant lattices observed with STM.

We also report the first observation of a third periodic pattern, a "supergiant lattice," superimposed on the giant and atomic lattices. In addition, the anomalous giant lattices may be a unique system for adsorption of clusters because their lattice constants are comparable with the size of clusters. On one of our samples, cobalt was deposited and cobalt clusters were imaged together with the giant lattice. This allows us to determine the adsorption sites of clusters on the giant lattice.

4.2   Experiment

The four graphite samples which we used were prepared independently. The first sample was cleaved in a high vacuum (2×10^{-8} torr) chamber. A small amount of cobalt was evaporated onto the surface leading to the formation of cobalt particles. These particles were of size 1 nm - 5 nm and were randomly distributed on the surface. Then the sample was transferred to a STM,[11] mounted in an ultra-high vacuum (5×10^{-10} torr) chamber, without breaking vacuum. The images were obtained in ultra-high vacuum at room temperature using a Pt-Ir tip. The tunneling current was kept at 4.5 nA and the bias voltage was varied from -500 mV to 200 mV.

The second sample was cleaved in air and then transferred to a STM[12] operating at ambient condition. The images were obtained with a silicon tip at positive tip bias voltage of 2.5 V and tunneling current of 4.6 nA.

The third sample was prepared in a high vacuum (2×10^{-7} torr) chamber by vapor deposition of cobalt on a freshly cleaved graphite substrate, similar as for the first sample. After deposition it was analyzed by x-ray photoelectron spectroscopy (XPS), which showed a coverage of less than 5% of a cobalt monolayer on the graphite surface. The STM images were taken in air at room temperature with a Pt-Ir tip at positive tip bias voltage of 54 mV and tunneling current of 1.8 nA.

The fourth sample was also prepared in a similar way as for the first sample except that, instead of cobalt, a small amount of carbon was deposited onto the surface. The STM images were taken in ultra-high vacuum at room temperature with a Pt-Ir tip. The bias voltage and tunneling current were maintained around 120 mV and 2 nA respectively.

For all four samples, the STMs were operated at constant height mode where the tip was maintained at a constant separation from the surface, and the variation of the tunneling current was recorded. The STM images presented in this paper were all taken from the first sample except that Figure 4.4 was taken from the fourth sample.

4.3   Results and Discussion

4.3.1 Giant Lattice

Figure 4.1 shows a large-scale STM image taken from the first sample. A sharp boundary which appears as a straight array of highlighted bright spots divides the image into two parts. The region on the right side of the boundary exhibits a hexagonal giant lattice with lattice constant of 3.8 nm. On the left side of the boundary, images at atomic scale were taken. They showed a regular graphite atomic structure. The giant

lattice extended over an area of at least 500 nm X 500 nm and was very stable. The variation in the bias voltage from -500 mV to 200 mV did not cause any significant change in the images.

A closer view of the giant lattice in Figure 4.1 is displayed in Figure 4.2(a). In a unit cell shown as the hexagon in the figure, there are three different sites which appear similar to the sites in the atomic image of graphite. The white spots at three corners of the hexagon resemble the β-sites in the atomic lattice and the gray areas at the other three corners resemble the α-sites. The dark area at the center of the hexagon resembles the hole-site. This can be seen in Figure 4.2(b) where a section is taken along the line AB indicated in Figure 4.2(a). We use g-h-site, g-α-site and g-β-site as notations for the "hole-site," "α-site" and "β-site" in the giant lattice respectively, to distinguish them from those in the atomic lattice. The giant corrugation is 1.2 - 1.4 nm and the atomic corrugation is 0.2 - 0.3 nm, both in respect to their hole-sites.

An even closer view, with atomic resolution, is shown in Figure 4.3. The angle between the giant and atomic lattices is ~ 28°. The atomic rows in the lattice appear twisted, especially along the direction which has the smallest angle to the scan line (horizontally from left to right). This twisting can be reduced significantly by changing the scan parameters such as increasing the scan rate and scan size or decreasing the feedback gains. Therefore the enhanced twisting along that direction is most likely a scan effect due to the high corrugation amplitude of the giant lattice.

The giant lattices observed on the other samples were also of hexagonal symmetry but with different lattice constant of 6.6 nm, 1.7 nm and 2.8 nm. They were rotated about 27° - 28° relative to the atomic orientation and extended over a region of up to a few hundred nanometers.

The corrugation was typically 4 - 5 times stronger compared to the atomic corrugation. The sharp boundaries which were observed in all cases suggest that grain boundaries or steps on the graphite surface may have existed, separating giant from regular lattices.

The suggestion of rotational Moire patterns,[5] in principle, is a reasonable approach because: (1) it provides a good explanation for the observed various superperiodicities; (2) the weak coupling between graphite layers could facilitate such small rotations of the top layer. However, direct observation of a rotated top layer relative to the underlying graphite has not been obtained in any of the STM studies of giant lattices. This is because electron tunneling with the STM occurs only between the tip and the first layer of graphite, and the atoms in deeper layers can not be observed.

Near a boundary, however, it is possible for the STM to image atomic lattices of graphite on both sides of the boundary simultaneously. The orientation of the two lattices can be compared to find out whether there exists a misorientation, and if so, whether the misorientational angle is related to the observed giant lattice. Figure 4.4 shows such an image taken from the fourth sample. The boundary is shown as indicated by the arrows on top and bottom of the image. The region on the left side of the boundary shows a giant lattice with lattice constant of 2.8 nm, while on the right side is the regular graphite lattice. In order to image the atomic lattices, we increased the bias voltage relatively. As a result, the giant lattice on the left is not clear in this image. Also, it is not clear if the boundary is associated with an atomic step or a grain boundary because superstructures of graphite are dominant at the boundary and extend to a few nanometers next to the boundary. Such superstructures are frequently

found on graphite near steps, grain boundaries, or any defects on the surface. They are attributed to periodic charge-density modulations induced by defects on the graphite surface,[4] as discussed in the previous chapter. Despite the superstructures of graphite, the atomic lattices on both sides of the boundary are clearly seen and are misoriented by ~ 5° as indicated in Figure 4.4. For two lattices of spacing d misoriented by an angle θ, the period D of the produced Moire pattern is given by an expression $D = d/[2\sin(\theta/2)]$.[5] Substituting d = 0.245 nm and θ = 5° into the above equation, we get D ≈ 2.8 nm. This value is in good agreement with the measured lattice constant, 2.8 nm, of the giant lattice. Therefore it provides a strong evidence that the observed giant lattices are due to misorientations of the graphite top layer.

However, since the STM sees only the top layer and is unable to reveal a pattern which is formed by two overlaid lattices,[13] the giant lattices observed with STM do not directly correspond to Moire patterns. In the following text we show that, although the atoms in deeper layers are not imaged, they may influence the apparent structure of the surface in the STM images. We concentrate on three structural aspects to account for such influences.

A. Symmetry of the Giant Lattices

Graphite is a layered material and carbon atoms in each layer form a honeycomb structure. The single crystal of graphite is formed by a ABAB... stacking of these layers, where every other layer is laterally shifted by one nearest neighbor distance. Figure 4.5(a) shows a schematic drawing of the surface of graphite. The structure of the surface is composed of two hexagonal lattices: an α sublattice consisting of atoms

with neighbors directly below in the next layer; and a β sublattice consisting of atoms without such neighbors. A side view cut along the direction indicated by the arrow is shown in the inset.

If the top layer is slightly rotated, the regular ABAB... stacking of graphite layers becomes CABAB..., where C is used as notation for the rotated top layer. A Moire pattern can be produced by overlapping the C-layer onto the next A-layer. Since the distinction between α and β sites is due to the ABAB... stacking, the C-layer is considered to be a honeycomb lattice without such a distinction. The resulting Moire pattern with C-layer rotated ~ 3.5° is shown in Figure 4.5(b). It displays a giant honeycomb structure, as indicated by the six large circles. The regions in the large solid circles are different from those in the large dashed circles. In the large solid circles, each α atom in the A-layer is covered or partially covered by an atom in the C-layer. In the large dashed circles, each β atom in the A-layer is covered or partially covered by an atom in the C-layer. Therefore the difference comes from the distinction between the α and β sites in the A-layer. Similar to the atomic structure of the graphite surface, the large honeycomb structure of the Moire pattern is composed of two hexagonal lattices: a sublattice represented by the large dashed circles; and another sublattice represented by the large solid circles. The giant honeycomb forms a unit cell of the Moire pattern. We call the center of the large dashed circles "M-α-sites," the center of the large solid circles "M-β-sites" and the center of the giant honeycomb "M-h-site". Therefore, the Moire pattern in Figure 4.5(b) displays a hexagonal symmetry with three different sites in a unit cell. Such a symmetry comes from the distinction between α and β sites of the second layer and is consistent with the symmetry of the observed giant lattices in STM images. For example, in

Figure 4.2(a), there are three different sites with different intensities in a unit cell of the giant lattice. In the next part, we will show how the M-α, M-β and M-h sites in a Moire pattern correspond to the g-α, g-β and g-h sites in a giant lattice respectively.

B. Atomic Sublattice in the Presence of the Giant Lattice

Although α and β atoms are geometrically identical at a regular graphite surface, β atoms appear at a higher intensity than α atoms in STM images. The asymmetry in the apparent intensity of the α and β atoms is due to their distinction resulting from the ABAB... stacking of graphite layers. Each α atom in the top layer sits directly above an α-site in the second layer, while each β atom sits above a hole-site. This leads to the difference in their electronic states. The β atoms have a higher density of states in the energy range scanned by the STM and therefore appear brighter in STM images.[3]

In the case where the top layer is rotated, the situation becomes much more complicated. As is shown in Figure 4.5(b), an atom in the top layer can find itself above any site in the second layer. For example, it can be above a hole-site, an α-site, a β-site, or anywhere in between these sites. For an atom above a hole-site, it would show maximum intensity in the STM images just like β atoms in a regular graphite lattice. Similarly an atom above an α-site would show less intensity and an atom above a β-site would show the least intensity.

With such an order of intensity in mind, we are now able to look closely at the M-h-sites, M-α-sites and M-β-sites in the Moire pattern. In a region at the M-h-site, atoms of the top layer are either above α-sites of the next layer or above β-sites. Those above the α-sites give higher intensity in

the STM images and form a hexagonal lattice. In a region at the M-α-site (M-β-site), atoms of the top layer are either above hole-sites of the next layer or above β-sites (α-sites). The atoms above the hole-sites give higher intensity in the STM images and also form a hexagonal lattice. Therefore a hexagonal atomic lattice is expected throughout all three regions in the Moire pattern. This is in good agreement with the observed atomic structure in actual STM images. In Figure 4.3, for example, a hexagonal atomic lattice is seen all over the image despite the presence of the giant lattice.

In addition to the atomic lattice, the regions at M-β-sites of the Moire pattern should give the highest average intensity than other regions. They correspond to g-β-sites of a giant lattice in STM images as, for example, Figure 4.2. Similarly the regions at M-α-sites give the next high intensity on average and the regions at M-h-sites give the minimum average intensity. They correspond to g-α-sites and g-h-sites of a giant lattice in STM images respectively.

C. Orientation of the Giant Lattice Relative to the Atomic Lattice

The orientation of the giant lattice relative to the atomic lattice provides additional information as to whether a misoriented top layer would be the cause of the giant lattice. If the observed giant lattices are due to small misorientations of the top layer, their orientation relative to the atomic lattice should be consistent with that predicted by the rotational Moire patterns. For a giant lattice with lattice constant in the range of 1.7 - 6.6 nm, the corresponding misorientational angle θ should be 3° - 6°. The orientation of the giant lattice relative to the atomic lattice is then 30°−θ/2,

6 2

i.e. 27° - 28.5°. This is also in perfect agreement with the observed orientation of giant lattices relative to the atomic lattice.

From the discussion on the three structural aspects, we have shown that all the features of giant lattices observed with STM can be explained by small misorientations of the top layer relative to the underlying graphite. The causes of such misorientations of the top layer are not known and may come from various processes such as cleavage or some peculiarity in the growing process of graphite. In addition, the superperiodicity introduced by a misoriented the top layer may also induce an electronic redistribution, which leads to the very high corrugation of the giant lattice compared to the atomic corrugation. A theoretical calculation of such an electronic redistribution is needed to be compared with the experimental results.

4.3.2 Supergiant Lattice

In addition to the giant and atomic lattices, a supergiant lattice was also observed on the first sample. Figure 4.6 is a contour STM image showing such a supergiant lattice. It appears on the right side of a boundary similar to that of Figure 4.1 and is superimposed on the giant lattice. It exhibits distorted hexagonal pattern with a periodicity of ~ 14 nm. The corrugation amplitude is ~ 0.1 nm, much less than the corrugation amplitude of the giant lattice. The supergiant pattern appeared in a number of images and scaled with various scan sizes. It was found only in the region where the giant lattice was observed, for example, only on the right side of the boundary in Figure 4.6.

The physical mechanism of such a supergiant lattice is not understood. It could be a result of the strain produced by the small rotation of the top layer.[14]

4.3.3   Adsorption Sites of Cobalt clusters

Since cobalt was also deposited on the first sample, small cobalt clusters were found occasionally on the surface together with the giant lattice. Figure 4.7(a) shows an image of a single cobalt particle of size 1 nm - 1.5 nm. It appears as the bright spot at the center of the image. Figure 4.7(b) is an image of two cobalt particles of similar size. In both images the cobalt particles were found on the top sites (g-β-sites) of the giant lattice. This is very similar to the observation of single atoms and atomic dimers of noble metals on the surface of graphite. They were mostly found at the top sites (β-sites) of the graphite atomic lattice.[15, 16] Single atoms and atomic dimers prefer β-sites in the atomic lattice because the β-sites have a higher local density of states at the Fermi level than the other sites. For cobalt particles, their much larger size makes it impossible to be bonded to any atomic site. But the presence of the giant lattice provides a similar environment as that of the atomic lattice to single atoms and dimers. For the same reason, the cobalt particles locate themselves on g-β-sites. This suggests that high local density of states at the Fermi level may determine the adsorption sites for both atoms and clusters.

4.4   Conclusions

Anomalous giant lattices have been observed on four graphite samples with scanning tunneling microscopy. They exhibit hexagonal

symmetry with lattice constants of 1.7 nm, 3.8 nm and 6.6 nm. Atomic resolution of graphite was obtained simultaneously. The various giant lattices are due to small misorientations of the top layer relative to the underlying graphite single crystal and their detailed features displayed in the STM images can be explained accordingly.

In addition, a supergiant lattice superimposed on the giant and atomic lattices has also been observed. It showed a distorted hexagonal pattern with a periodicity of ~ 15 nm. The causes of the supergiant lattice is not clear and may be due to the strain produced by the small rotation of the top layer.

Cobalt clusters adsorbed on the surface were also imaged together with the giant lattice. They were found to prefer top sites of the giant lattice, suggesting that high local density of states at the Fermi level may determine the adsorption sites.

4.5   References

1. J. M. Soler, A. M. Baro, and N. Garcia, Phys. Rev. Lett. **57**, 444 (1986).

2. J. Tersoff, Phys. Rev. Lett. **57**, 440 (1986).

3. D. Tomanek, S. G. Louie, H. J. Mamin, D. W. Abraham, R. E. Thomson, E. Ganz, and J. Clarke, Phys. Rev. B **35**, 7790 (1987).

4. J. Xhie, K. Sattler, U. Muller, N. Venkateswaran, and G. Raina, Phys. Rev. B **43**, 8917 (1991).

5. M. Kuwabara, D. R. Clarke, and D. A. Smith, Appl. Phys. Lett. **56**, 2396 (1990).

6. J. W. Lyding, J. S. Hubacek, G. Gammie, S. Skala, and R. Brockenbrough, J. Vac. Sci. Technol. A **6** (2), 363 (1988).

7. T. Hashizume, I. Kamiya, Y. Hasegawa, N. Sano, T. Sakurai, and H. W. Pickering, J. Microsc. **152**, 347 (1988).

8. V. Elings and F. Wudl, J. Vac. Sci. Technol. **A6**, 412 (1988).

9. J. E. Buckley, J. L. Wragg, and H. W. White, J. Vac. Sci. Technol. B **9** (2), 1079 (1991).

10. P. I. Oden, T. Thundat, L. A. Nagahara, S. M. Lindsay, G. B. Adams, and O. F. Sankey, Surf. Sci. Lett. **254**, L454 (1991).

11. McAllister Technical Services, Coeur d'Alene, Idaho, USA.

12. Digital Instruments, Inc., Santa Barbara, California, USA.

13. When a double-tip was scanning over different grains in the vicinity of a grain boundary, the STM images showed Moire patterns. Such Moire patterns were contributed to simultaneous imaging of the double-tip. T. R. Albrecht, H. A. Mizes, J. Nogami, S.-I. Park, and C. F. Quate, Appl. Phys. Lett. **52**, 362 (1988).

14. O. L. Alerhand, D. Vanderbilt, R. D. Meade, and J. D. Joannopoulos, Phys. Rev. Lett. **61**, 1973 (1988).

15. E. Ganz, K. Sattler, and J. Clarke, Phys. Rev. Lett. **60**, 1856 (1988).

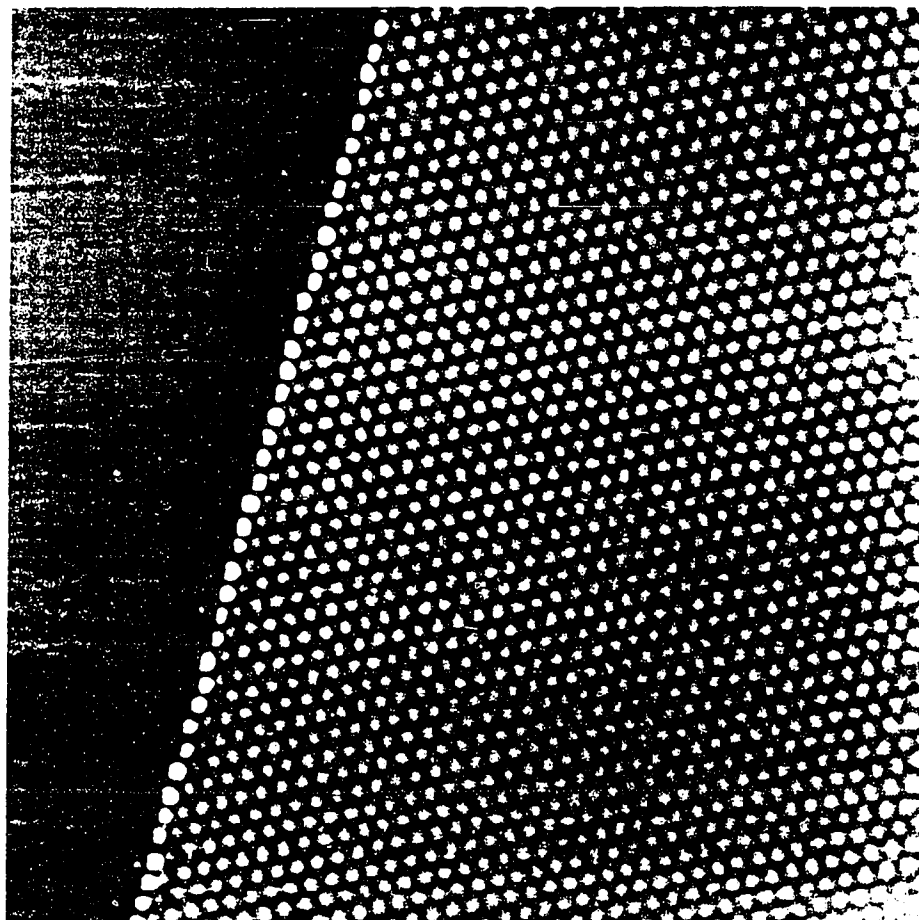16. U. Muller, K. Sattler, J. Xhie, N. Venkateswaran, and G. Raina, J. Vac. Sci. Technol. B **9** (2), 829 (1991).

Figure 4.1: A STM image (160 nm × 160 nm) showing a sharp boundary which separates the giant lattice from regular graphite. The giant lattice on the right side of the boundary exhibits a hexagonal symmetry with lattice constant of 3.8 nm.
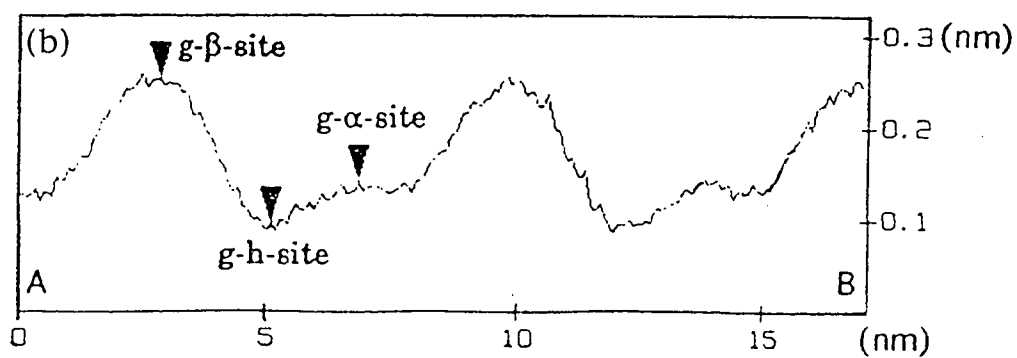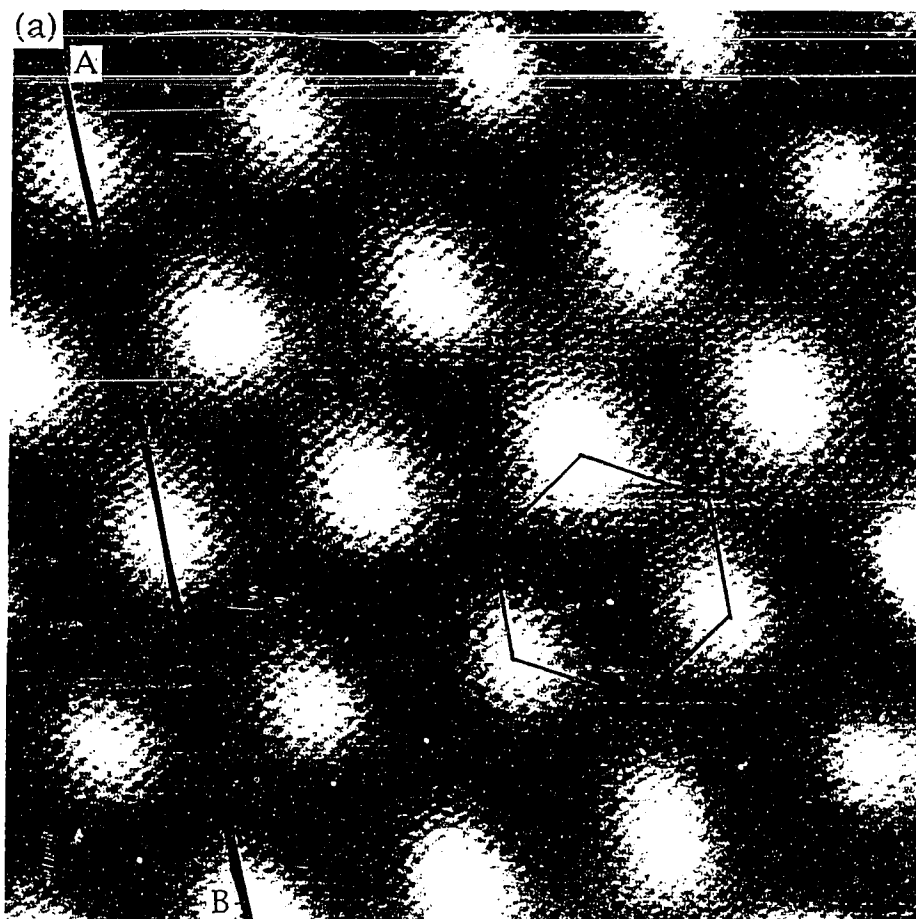
Figure 4.2: (a) A closer view (17 nm × 17 nm) of the giant lattice in Figure 4.1. The hexagon shows a unit cell of the giant lattice. (b) A height plot along the line AB indicated in (a).
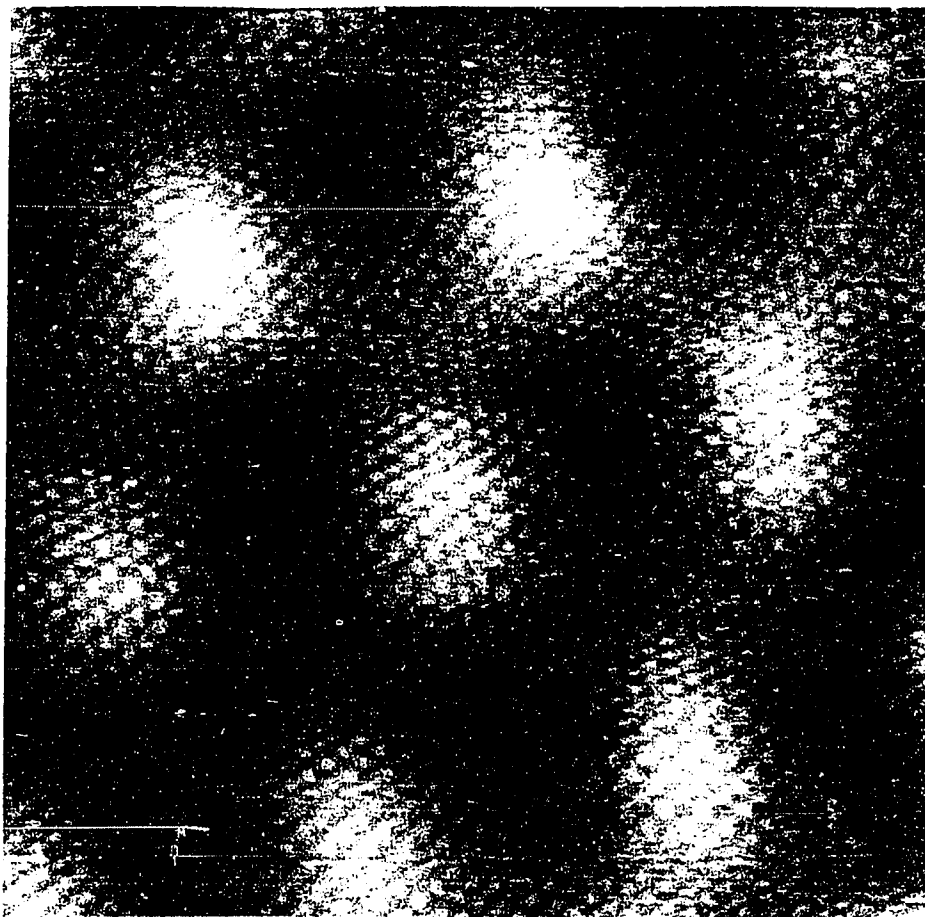
Figure 4.3:   A STM image (10 nm × 10 nm) showing both the giant and atomic lattices.

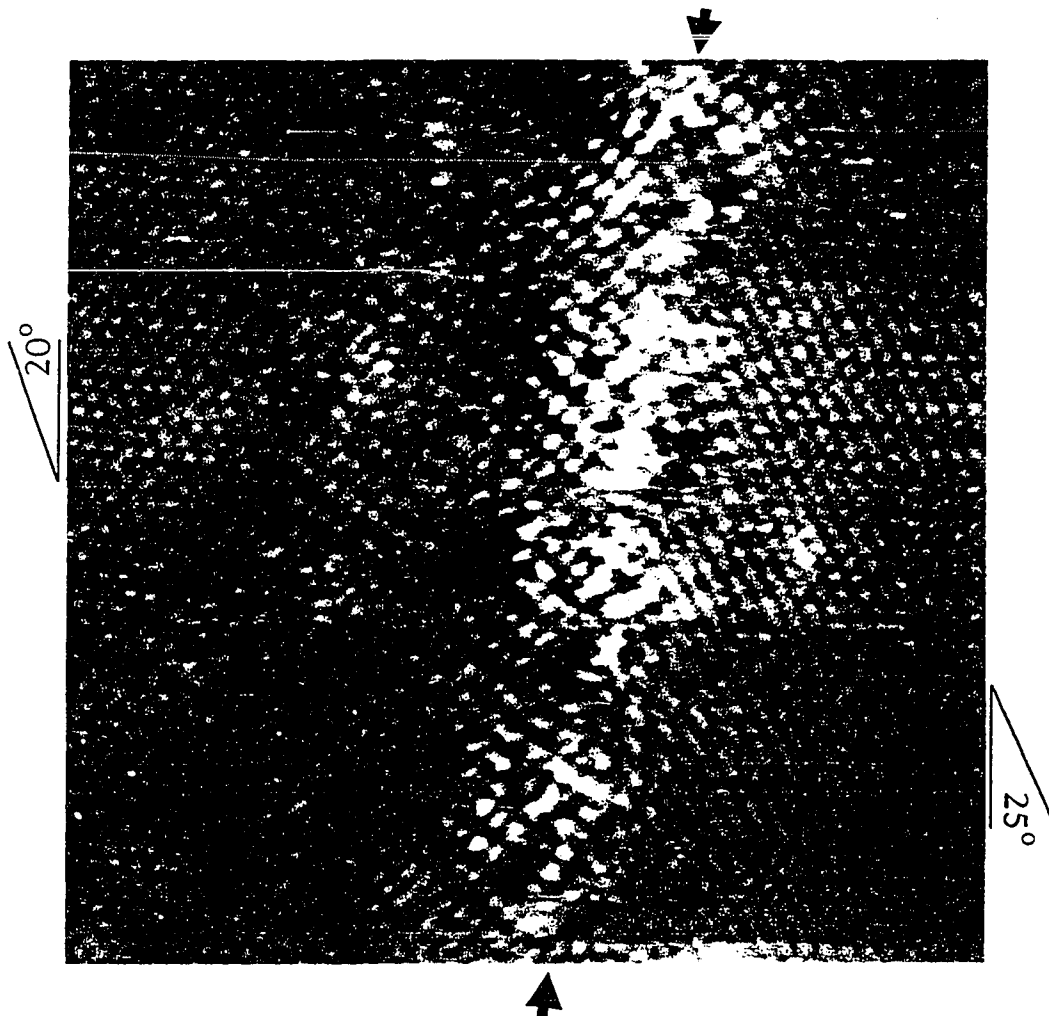Figure 4.4: A STM image (11 nm × 11 nm) taken near a boundary of the giant lattice (left) with lattice constant of 2.8 nm. The atomic lattices on both sides of the boundary are clearly seen and are misoriented relatively to each other by ~ 5°. The bias voltage was kept relatively high in order to image the atomic lattices. As a result, the giant lattice on the left is not clear in this image. The superstructures near the boundary are due to periodic charge-density modulations discussed in Chapter 3.
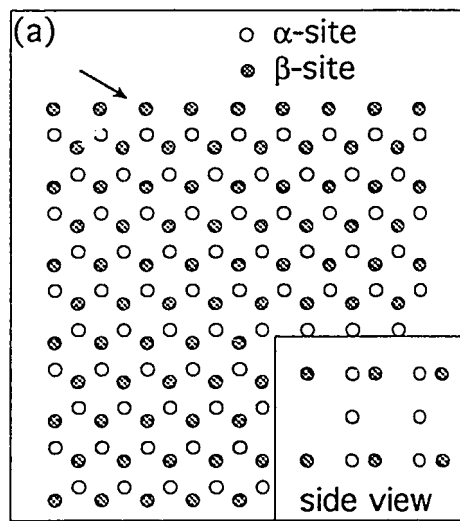
Figure 4.5(a): Schematic drawing of the surface structure of graphite.

The inset shows a side view cut along the arrow.
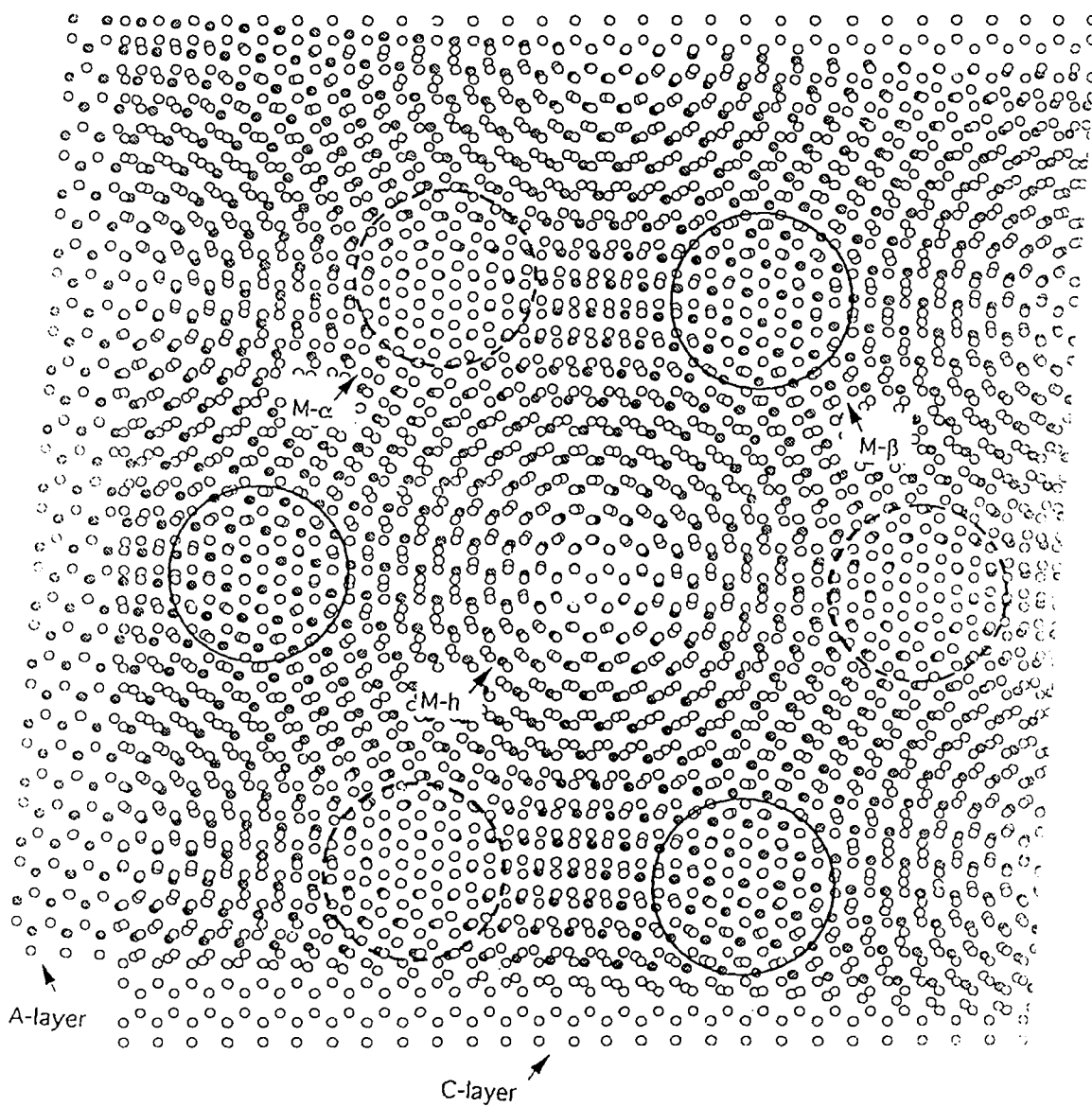
Figure 4.5(b): A Moire pattern produced by overlapping two lattices. One of them (C-layer) has a honeycomb structure and the other (A-layer) has the structure shown in (a). The two lattices are rotated relatively to each other by 3.5°.
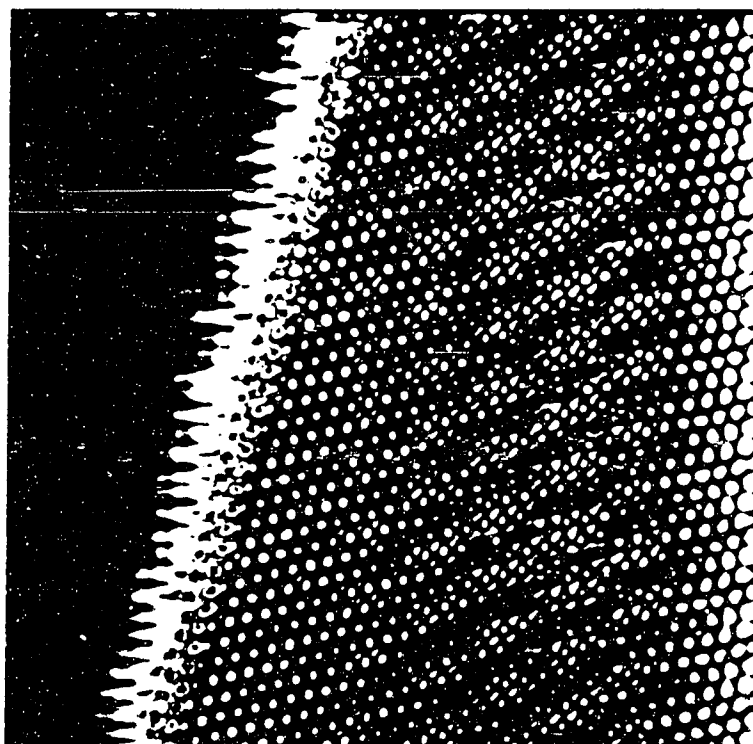
Figure 4.6: A contour STM image (160 nm X 160 nm) similar to Figure 4.1. The region at the right side of the boundary shows a supergiant lattice superimposed on the giant lattice. The corrugation of the super lattice is extremely small, ~ 1/10 of the corrugation of the giant lattice. In order to bring out the effect, high contrast contour scale is used, which also leads to the bright bands at the boundary.

Figure 4.7: (a) STM image (38 nm × 38 nm) showing a single cobalt particle adsorbed on the giant lattice with lattice constant of 3.8 nm. (b) STM image (38 nm × 38 nm) showing two cobalt particles adsorbed on the giant lattice.

Chapter V

CONCLUDING REMARKS

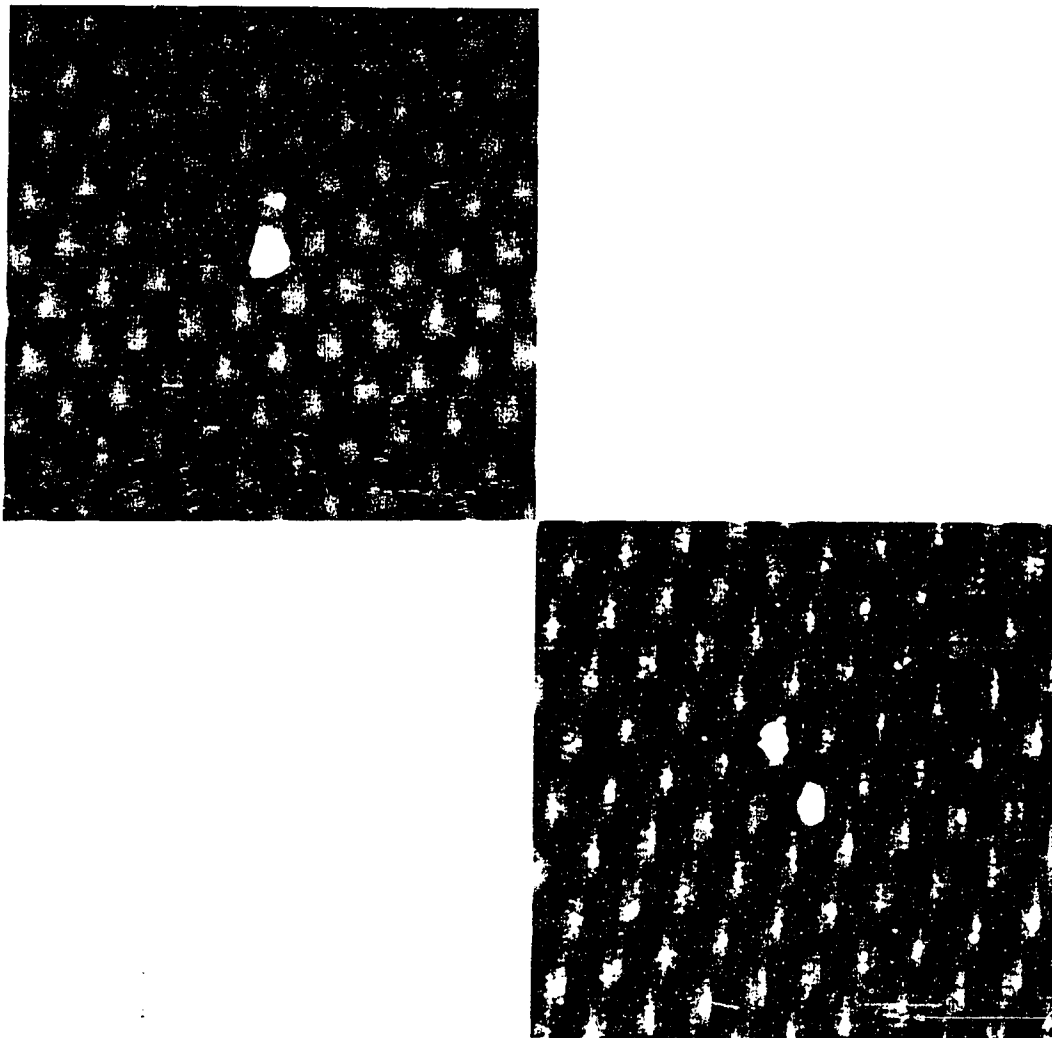This PhD research is inspired by the need of understanding the physics of supported clusters and is directed toward obtaining local structural information of the clusters and the substrates using scanning tunneling microscope.

First, we performed a topographic study of adatoms and small clusters of platinum on highly-oriented pyrolytic graphite both in air and in ultra-high vacuum. Taking the graphite lattice as reference, we determined cluster structures as well as their orientational and positional registry with the graphite lattice. In addition a statistical study has been performed to obtain distributions of adsorption sites and bond lengths. We find that a platinum single atom tends to bind to the β-site of the graphite lattice, but has also a high probability to bind at any other sites. For dimers the average bond distance is ~0.246 nm which is very close to the graphite lattice constant. The trimer bond length is 0.261 nm, suggesting that the Pt-Pt interaction is dominant.

For many adsorbed clusters (platinum and cobalt) on graphite, various superstructures of graphite were found in the nearby regions. The superstructures were localized in small areas near defects and decayed within a distance of 2 - 5 nm into the graphite lattice. They can be explained by periodic charge-density modulation superimposed onto the graphite lattice. These periodic modulations have a period of 1.5a (a = 0.245 nm, is the lattice constant of graphite) and exist in three possible directions, each rotated 30° relative to the graphite lattice. They are

generated by adsorbed clusters which perturb the surface charge-density. Images of the superstructures depend on the dominant periodic charge density modulations and their relative intensities and phases with respect to underlying graphite lattice. The cluster-induced modulations may have an effect on the atomic arrangements in the clusters. Atoms in clusters tend to bind to those sites which have maximum intensity of the modulation.

Among many samples of graphite substrate being studied, anomalous giant lattices were observed on four of the samples. They exhibit hexagonal symmetry with lattice constants of 1.7 nm, 2.8 nm, 3.8 nm and 6.6 nm. Atomic resolution of graphite was obtained simultaneously. By introducing small rotations of the top graphite layer relative to the underlying single crystal, a complete description is developed to account for all the features displayed by the STM images. In addition, a supergiant lattice superimposed on the giant and atomic lattices has also been observed. It showed a distorted hexagonal pattern with a periodicity of ~ 15 nm. The causes of the supergiant lattice is not clear and may be due to the strain produced by the small rotation of the top layer. Cobalt clusters on the surface were also imaged together with the giant lattice. They were found to prefer top sites of the giant lattice, suggesting that high local density of states at the Fermi level may determine the adsorption sites.

The study of clusters and their interaction with the substrate is of fundamental importance in future technologies such as catalysis, microelectronics and material science. The investigation of small clusters can lead to advanced engineering technology for novel industrial devices, for example, in the miniaturization of electronic components and their

fabrication. The development of new processes based on cluster research can give new materials with improved properties such as super-strength and ultra-light weight.

BIBLIOGRAPHY

Albrecht, T. R., Mizes, H. A., Nogami, J., Park, S.-I., and Quate, C. F.,
Appl. Phys. Lett. **52**, 362 (1988).

Alerhand, O. L., Vanderbilt, D., Meade, R. D., and Joannopoulos, J. D.,
Phys. Rev. Lett. **61**, 1973 (1988).

Allan, G., and Lannoo, M., Phys. Rev. Lett. **66**, 1209 (1991).

Apai, G., Hamilton, J. F., Stohr, J., and Thompson, A., Phys. Rev. Lett. **43**,
165 (1979).

Bardeen, J., Phys. Rev. Lett. **6**, 57 (1961).

Binnig, G., Rohrer, H., Gerber, Ch., and Weibel, E., Phys. Rev. Lett. **49**, 57
(1982).

Buckley, J. E., Wragg, J. L., and White, H. W., J. Vac. Sci. Technol. B **9** (2),
1079 (1991).

Coleman, R. V., Giambattista, B., Hansma, P. K., Johnson, A., McNairy,
W. W., and Slough, C. G., Adv. Phys. **37**, 559 (1988).

Elings, V., and Wudl, F., J. Vac. Sci. Technol. A**6**, 412 (1988).

First, P. N., Stroscio, J. A., Dragoset, R. A., Pierce, D. T., and Celotta, R.
J., Phys. Rev. Lett. **63**, 1416 (1989).

Ganz, E., Sattler, K., and Clarke, J., J. Vac. Sci. Technol. A **6**, 419 (1988).

Ganz, E., Sattler, K., and Clarke, J., Phys. Rev. Lett. **60**, 1856 (1988).

Ganz, E., Sattler, K., and Clark, J., Surf. Sci. **219**, 33 (1989).

Hashizume, T., Kamiya, I., Hasegawa, Y., Sano, N., Sakurai, T., and
Pickering, H. W., J. Microsc. **152**, 347 (1988).

Hilf, E. R., Kammer, F., and Wien, K., "PDMS and Clusters," Springer
(1986).

Iijima, S., and Ichihashi, T., Phys. Rev. Lett. **56**, 616 (1986).

Jena, P., Rao, B. K., and Khanna, S. N., "Physics and Chemistry of Small Clusters," NATO ASI Series B: Physics Vol. **158**, Plenum Press (1987).

Kellog, G. L., Surf. Sci. **187**, 153 (1987).

Kuk, Y., Jarrold, M. F., Silverman, P. J., Bower, J. E., and Brown, W. L., Phys. Rev. B **39**, 11168 (1989).

Kuwabara, M., Clarke, D. R., and Smith, D. A., Appl. Phys. Lett. **56**, 2396 (1990).

Lyding, J. W., Hubacek, J. S., Gammie, G., Skala, S., and Brockenbrough, R., J. Vac. Sci. Technol. A **6** (2), 363 (1988).

Martensson, P., and Feenstra, R. M., J. Microsc. **152**, 761 (1988).

Mizes, H. A., and Foster, J. S., Science **244**. 559 (1989).

Mizes, H. A., Park, S.-I., and Harrison, W. A., Phys. Rew. B **36**, 4491 (1987).

Mo, Y.-W., Savage, D. E., Swartzentruber, B. S., and Lagally, M. G., Phys. Rev. Lett. **65**, 1020 (1990).

Montano, P. A., Schulze, W., Tesche, B., Shenoy, G. K., and Morrison, T. I., Phys. Rev. B **30**, 672 (1984).

Montano, P. A., Shenoy, G. K., Alp, E. E., Schulze, W., Urban, J., Phys. Rev. Lett. **56**, 2076 (1986).

Montano, P. A., Zhao, J., Ramanathan, M., Shenoy, G. K., Schulze, W., and Urban, J., Chem. Phys. Lett. **164**, 126 (1989).

Muller, U., Sattler, K., Xhie, J., Venkateswaran, N., and Raina, G., J. Vac. Sci. Technol. B **9** (2), 829 (1991).

Nakagawa, Y., Bando, H., Ono, M., and Kajimura, K., "$\sqrt{3}\times\sqrt{3}$ Structure on Graphite Surface," unpublished.

Oden, P. I., Thundat, T., Nagahara, L. A., Lindsay, S. M., Adams, G. B., and Sankey, O. F., Surf. Sci. Lett. **254**, L454 (1991).

79

Rabe, J. P., Sano, M., Batchelder, D., and Kalatchev, A. A., Journal of Microscopy **152**, 573 (1988).

Raghavan, K., Stave, M. S., and DePristo, A. E., J. Chem. Phys. **91**, 1904 (1989).

Raina, G., Sattler, K., Muller, U., Venkateswaran, N., and Xhie, J., J. Vac. Sci. Technol. B **9** (2), 1039 (1991).

Rizzetti, A., Xhie, J., Sattler, K., Yamamoto, D., and Pong, W., J. of Electron Spectrosc. Relat. Phenom. **58**, 359 (1992).

Sands, D., "Introduction to Crystallography," Benjamin-Cummings, Reading, Mass. (1969).

Smith, D. P. E., and Elrod, S., Rev. Sci. Inst. **56**, 1970 (1985).

Soler, J. M., Baro, A. M., and Garcia, N., Phys. Rev. Lett. **57**, 444 (1986).

Sugano, S., Nishina, Y., and Ohnishi, S., "Microclusters," Springer Series in Materials Science **4**, Springer (1987).

Tersoff, J., Phys. Rev. Lett. **57**, 440 (1986).

Tersoff, J., and Hamann, D. R., Phys. Rev. B **31**, 805 (1985).

Tomanek, D., Louie, S. G., Mamin, H. J., Abraham, D. W., Thomson, R. E., Ganz, E., and Clarke, J., Phys. Rev. B **35**, 7790 (1987).

Traeger, F., and zu Putltz, G., "Metal Clusters," Springer (1986).

Trafas, B. M., Hill, D. M., Benning, P. J., Waddill, G. D., Yang, Y.-N., Siefert, R. L., and Weaver, J. H., Phys. Rev. B **43**, 7174 (1991).

Upton, T. H., Phys. Rev. Lett. **56**, 2168 (1986).

Venables, J. A., Derrien, J., and Janssen, A. P., Surf. Sci. **95**, 441 (1980).

Xhie, J., Sattler, K., Muller, U., Venkateswaran, N., and Raina, G., Phys. Rev. B **43**, 8917 (1991).